

UNIVERSITY OF WARMIA AND MAZURY IN OLSZTYN

Technical Sciences

23(4) 2020

Editorial Board

Ceslovas Aksamitauskas (Vilnius Gediminas Technical University, Lithuania), Olivier Bock (Institut National de L'Information Géographique et Forestière, France), Stefan Cenkowski (University of Manitoba, Canada), Adam Chrzanowski (University of New Brunswick, Canada), Davide Ciucci (University of Milan-Bicocca, Italy), Sakamon Devahastin (King Mongkut's University of Technology Thonburi in Bangkok, Thailand), German Efremov (Moscow Open State University, Russia), Mariusz Figurski (Military University of Technology, Poland), Maorong Ge (Helmholtz-Zentrum Potsdam Deutsches GeoForschungsZentrum, Germany), Dorota Grejner-Brzezinska (The Ohio State University, USA), Janusz Laskowski (University of Life Sciences in Lublin, Poland), Arnold Norkus (Vilnius Gediminas Technical University, Lithuania), Stanisław Pabis (Warsaw University of Life Sciences-SGGW, Poland), Lech Tadeusz Polkowski (Polish-Japanese Institute of Information Technology, Poland), Arris Tijsseling (Technische Universiteit Eindhoven, Netherlands), Vladimir Tilipalov (Kaliningrad State Technical University, Russia), Alojzy Wasilewski (Koszalin University of Technology, Poland)

Editorial Committee

Marek Markowski (Editor-in-Chief), Piotr Artiemjew, Kamil Kowalczyk, Wojciech Sobieski, Piotr Srokosz, Magdalena Zielińska (Assistant Editor), Marcin Zieliński

Features Editors

Piotr Artiemjew (Information Technology), Marcin Dębowski (Environmental Engineering), Zdzisław Kaliniewicz (Biosystems Engineering), Grzegorz Królczyk (Materials Engineering), Marek Mróz (Geodesy and Cartography), Ryszard Myhan (Safety Engineering), Wojciech Sobieski (Mechanical Engineering), Piotr Srokosz (Civil Engineering), Jędrzej Trajer (Production Engineering)

Statistical Editor

Paweł Drozda

Executive Editor

Mariola Jezierska

The Technical Sciences is indexed and abstracted in BazTech (<http://baztech.icm.edu.pl>) and in IC Journal Master List (<http://journals.indexcopernicus.com>)

The Journal is available in electronic form on the web sites
<http://www.uwm.edu.pl/techsci> (subpage Issues)
<http://wydawnictwo.uwm.edu.pl> (subpage Czytelnia)

The electronic edition is the primary version of the Journal

PL ISSN 1505-4675

e-ISSN 2083-4527

© Copyright by Wydawnictwo UWM • Olsztyn 2020

Address

ul. Jana Heweliusza 14
10-718 Olsztyn-Kortowo, Poland
tel.: +48 89 523 36 61
fax: +48 89 523 34 38
e-mail: wydawca@uwm.edu.pl

Ark. wyd. 5,4, ark. druk. 4,5, nakład 75 egz.
Druk – Zakład Poligraficzny UWM, zam. 121

Contents

M. JANULIN – <i>Conditions for optimizing powertrain performance in a vehicle with an internal combustion engine</i>	291
S. KŁYSZ – <i>Investigation of low- and high-cycle fatigue in Al 2024-T4 alloy</i>	309
P. SZCZYGLAK – <i>Comparison of ploughing vs. Ploughless cultivation in terms of energy expenditure and treatment quality</i>	323
D. MIEDZIŃSKA – <i>Selection of material model of chosen photocurable resin for application in finite element analyses</i>	337



Quarterly peer-reviewed scientific journal

ISSN 1505-4675
e-ISSN 2083-4527

TECHNICAL SCIENCES

Homepage: www.uwm.edu.pl/techsci/



DOI: <https://doi.org/10.31648/ts.6069>

CONDITIONS FOR OPTIMIZING POWERTRAIN PERFORMANCE IN A VEHICLE WITH AN INTERNAL COMBUSTION ENGINE

Michał Janulin

ORCID: 0000-0003-3436-9079

Department of Vehicle and Machine Construction and Operation
Faculty of Technical Sciences
University of Warmia and Mazury in Olsztyn

Received 05 November 2020, accepted 16 December 2020, available online 17 December 2020.

Key words: optimization, powertrain, gear ratio, vehicle energy efficiency, fuel consumption.

Abstract

The paper presents optimization of the drive system in terms of adapting it to the characteristics of another engine. Powertrain parameters in a vehicle with an internal combustion engine were selected based on the following criteria: fuel consumption, engine dynamics, and emission standards for harmful substances. A light-duty passenger vehicle with gross vehicle weight rating (GVWR) of 3.5 tons was modified by replacing a spark-ignition engine with a diesel engine. The gear ratio in the powertrain had to be modified accordingly to optimize the engine's performance, enhance engine dynamics, minimize fuel consumption and toxic emissions. The optimization of selected parameters of the vehicle driveline was performed based on the requirements of the standard NEDC and WLTC cycles.

Correspondence: Michał Janulin, Katedra Budowy, Eksploatacji Pojazdów i Maszyn, Uniwersytet Warmińsko-Mazurski, ul. Michała Oczapowskiego 11, p. D2, 10-719 Olsztyn, e-mail: michal.janulin@uwm.edu.pl

Introduction

The design of new vehicles and the upgrading and adaptation of the existing vehicles require optimization techniques for reducing the time and cost of these operations. Optimization techniques also facilitate the search for trade-off solutions that account for different and often contradictory customer requirements.

The process of upgrading vehicles with internal combustion engines involves the reduction of engine capacity, improvement of the power-to-weight ratio, the introduction of turbochargers, cylinder deactivation systems and start-stop systems to minimize fuel consumption in urban traffic. FRASER et al. (2009) analyzed the extent to which a decrease in engine cylinder capacity reduces fuel consumption. The study was conducted on a D-segment car where a 2.0 L TGDI engine was replaced with a 1.2 L MAHLE engine. Driving cycle tests revealed a 15% decrease in fuel consumption.

The main goals of modern vehicle design, upgrade and operation are to reduce power consumption, increase energy efficiency and minimize vehicles' negative impact on the environment. These processes rely on optimization techniques that considerably reduce the time and cost of investments in the automotive industry. Optimization techniques are deployed to improve structural solutions in vehicles (FRIES et al. 2018, LI et al. 2020, OGLIEVE et al. 2017, WENCHEN et al. 2016) and to adapt vehicles to operational environments (BERTRAM, HERZOG 2013, SKUGOR, DEUR 2014, PENG et al. 2018).

To further the development of effective automotive solutions and modern powertrain systems, optimization techniques were used in this study to improve selected operating parameters of a vehicle with an internal combustion engine. Quality criteria, functional limitations and decision parameters need to be established to fully harness the potential of optimization techniques. Such analyses should also consider the operating conditions of vehicles and systems whose performance is determined by many interacting processes. The results of such studies can be used to identify the available scope for potential improvement in powertrain systems.

Analysis of a vehicle's operating parameters as optimization criteria

Criteria for evaluating a vehicle's energy consumption

A vehicle's energy consumption is measured in kWh. The volume of energy consumed per unit distance is determined in kWh/km, and the same measure can be applied to evaluate powertrain performance. In a vehicle with an internal combustion engine, energy consumption is normally expressed in terms of fuel

consumption per unit of distance, usually L/100 km (kg/100 km). The demand for energy in a vehicle with an internal combustion engine can be expressed with the use of the below formula (KROPIWNICKI 2011):

$$E = \int_0^{t_c} (F_{rf} \cdot V) dt \quad (1)$$

where:

- t_c – cycle time,
- F_{rf} – total resistive forces acting on a moving vehicle,
- V – vehicle's linear velocity.

The following resistive forces act on a vehicle:

- rolling friction F_f ,
- air resistance F_{air} ,
- gradient resistance F_g ,
- inertial resistance F_i ,
- internal resistance F_{int} .

Rolling friction can be described with the following formula:

$$F_f = f_r \cdot m \cdot g \cdot \cos \alpha = f \cdot Q_i \quad (2)$$

where:

- f_r – coefficient of rolling friction,
- m – vehicle mass,
- α – road gradient,
- Q_i – tire-ground interaction force.

Air resistance is calculated as follows (MITCHKE 1977):

$$F_{air} = \frac{c_x \cdot \rho_a \cdot A \cdot v^2}{2} \quad (3)$$

where:

- C_x – coefficient of aerodynamic resistance,
- ρ_a – air density,
- A – car frontal area,
- v – linear velocity.

Gradient resistance is determined based on the following formula:

$$F_g = m \cdot g \cdot \sin \alpha \quad (4)$$

Inertial resistance is associated with translational motion or rotational motion of an object (GILLESPIE 1992, MITCHKE 1977, ORZEŁOWSKI 1969). It is generally calculated with the use of the following equation:

$$F_i = m \cdot \delta \cdot \frac{dv}{dt} \quad (5)$$

where:

$\frac{dv}{dt}$ – linear acceleration,

δ – coefficient for converting the inertia of rotating components to the inertia of translational motion.

The sum of resistive forces:

$$F_{rf} = F_f + F_{air} + F_g + F_i \quad (6)$$

is used to determine instantaneous power demand:

$$P_r = F_{rf} \cdot V \quad (7)$$

The thrust force produced by the engine shaft and a vehicle's velocity can be expressed as follows (GILLESPIE 1992):

$$F_t = \frac{M \cdot i_g \cdot i_o \cdot \eta_t}{r_d} \quad (8)$$

$$V = \frac{\pi \cdot n \cdot r_d}{30 \cdot i_g \cdot i_o} \quad (9)$$

where:

M – torque,

n – rotational speed of the engine shaft,

i_g – gear ratio of the gear box,

i_o – gear ratio of the final drive,

r_d – dynamic rolling radius.

A vehicle's maximum velocity in a given driving environment can be determined with the use of the dynamic coefficient D which is calculated as follows:

$$D = \frac{F_t - F_{air}}{m \cdot g} \quad (10)$$

When the remaining resistive forces are considered, the equation can be expressed as follows:

$$D = f_r + w + \frac{\delta}{g} \cdot \frac{dv}{dt} \quad (11)$$

where w is the coefficient of gradient resistance: $w = \tan \alpha \approx \sin \alpha$. If the vehicle is moving on a flat roadway ($\alpha = 0$) at a constant speed ($\frac{dv}{dt} = 0$), then $D = f_r$, therefore:

$$\frac{F_t - F_{air}}{m \cdot g} = f_r \quad (12)$$

$$\frac{M \cdot i_g \cdot i_o \cdot \eta_t}{r_d} - \frac{c_x \cdot \rho_a \cdot A \cdot v^2}{2} = f_r \cdot m \cdot g,$$

$$v_{\max} = \sqrt{\frac{1}{C_x \cdot \rho_a \cdot A} \cdot \left(\frac{2M \cdot i_{g\min} \cdot i_o \cdot \eta_t}{r_d} - 2f_r \cdot m \cdot g \right)} \quad (13)$$

where:

$i_{g\min}$ – the gear ratio of the final gear.

The maximum slope that the vehicle can climb is calculated with the following formula:

$$w = D - f_r - \frac{\delta}{g} \cdot \frac{dv}{dt} \quad (14)$$

If the vehicle moves at a constant speed, then, therefore:

$$w = \frac{F_t - F_{\text{air}}}{m \cdot g} - f_r \quad (15)$$

The gear required to achieve the speed of V_f should be considered when calculating the acceleration of a vehicle with an internal combustion engine. If the last gear is required, and the vehicle has a five-speed gearbox, then the time needed to reach speed V_f can be calculated as follows:

$$t_a = \int_0^{V_1} \frac{m \cdot \delta}{\frac{P_t}{V_1} - m \cdot g \cdot f_r - 0.5 \cdot \rho_a \cdot C_x \cdot A \cdot V^2} dV + \int_{V_1}^{V_2} \frac{m \cdot \delta}{\frac{P_t}{V_2} - m \cdot g \cdot f_r - 0.5 \cdot \rho_a \cdot C_x \cdot A \cdot V^2} dV + \int_{V_2}^{V_3} \frac{m \cdot \delta}{\frac{P_t}{V_3} - m \cdot g \cdot f_r - 0.5 \cdot \rho_a \cdot C_x \cdot A \cdot V^2} dV +$$

$$\int_{V_3}^{V_4} \frac{m \cdot \delta}{\frac{P_t}{V_4} - m \cdot g \cdot f_r - 0.5 \cdot \rho_a \cdot C_x \cdot A \cdot V^2} dV + \int_{V_4}^{V_f} \frac{m \cdot \delta}{\frac{P_t}{V} - m \cdot g \cdot f_r - 0.5 \cdot \rho_a \cdot C_x \cdot A \cdot V^2} dV \quad (16)$$

where V_1, V_2, V_3, V_4 denote linear speeds at which the maximum engine power can be achieved in gears 1, 2, 3 and 4, respectively.

Vehicle simulation model

The presented formulas are used to model vehicles with various types of powertrain systems. All processes that describe a vehicle's motion have to be taken into account to solve optimization problems.

Research into new powertrain systems in the automotive industry contributed to the development of comprehensive driving simulators, in particular for analyzing the interactions between the system and its individual components (DABADIE et al. 2011, DA COSTA, ALIX 2011), describing the characteristics of various components (HUSAIN, ISLAM 1999), developing and validating control

algorithms and vehicle control systems (SCIARETTA et al. 2008, VERDONCK et al. 2010). A driving simulator developed based on the LMS IMAGINE.Lab AMESim® platform (<https://www.plm.automation.siemens.com/global/en/products/simcenter/simcenter-amesim.html>) is presented in Figure 1.

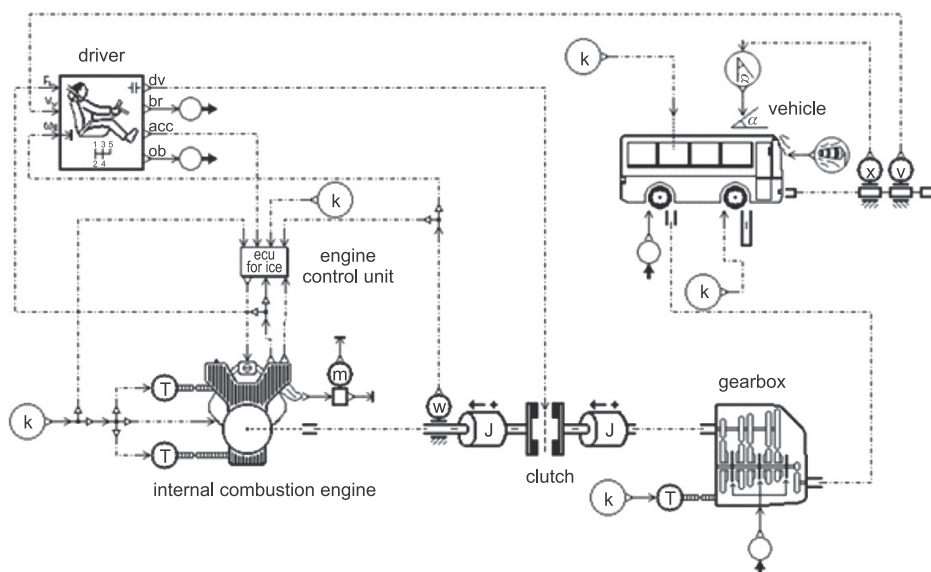


Fig. 1. Simulation model of a vehicle developed in the LMS.IMAGINE.Lab AMESim® environment

The specific character of the optimization procedure should also be considered, including iteration algorithms which can perform more than 1,000 individual calculations. Empirically determined characteristics of selected components in a model of a complex mechanical system can be used to reconcile model requirements with research assumptions and the accuracy of the results. In a simulation, the model of an internal combustion engine does not rely on known methods for calculating basic processes (HEYWOOD 1988). Engine parameters in the simulation model were described based on empirical data, including the speed characteristics of an internal combustion engine (GRYTSYUK, VRUBLEVSKIY 2018) and general engine characteristics.

The proposed model has considerable potential for analyzing the influence of structural and operating parameters on a vehicle's energy consumption, engine dynamics and compliance with emission standards.

Selection of driving cycles for the optimization problem

A detailed numerical description of tractive force and linear velocity in real-world driving conditions is relatively complex. Driving cycles that simulate a typical driving environment are developed to best represent real-world conditions. Depending on the aim of the analysis, driving cycles can simulate urban or extra-urban traffic, and they describe changes in the speed of a vehicle moving on a flat roadway. Various driving cycles have been developed for analyzing energy efficiency in vehicles (BARLOW et al. 2009, GIAKOURIS, ZACHOTIS 2017).

Until recently, the New European Driving Cycle (NEDC) was the mandatory driving cycle for assessing emission levels in passenger vehicles. The NEDC was developed in the late 1980s, and it does not fully reflect present traffic conditions, mostly due to changes in traffic intensity and the number of vehicles. The NEDC was designed to represent typical urban driving conditions, including idling (GIAKOURIS, ZACHOTIS 2017), which largely contributed to the development of start-stop systems. Moreover, the assumed acceleration values did not require high engine loads in modern vehicles, which prompted designers to downsize engines. The cycle was performed on a roller test bench at a temperature of 20-30°C.

The effectiveness of optimization is largely determined by the operating parameters of the powertrain. Vehicle performance is generally assessed in stationary mode or in test cycles. The WLTC driving cycle produces more accurate results, and a vehicle's real-world performance can be simulated with an accuracy of up to 80% (GIAKOURIS, ZACHOTIS 2017).

The performance of a four-cylinder 2 dm³ diesel engine in a class 3 vehicle was compared in the NEDC and the WLTC (Fig. 2), and the results indicate that engine characteristics are not easy to determine. Unlike in the NEDC, the engine operates in non-stationary mode during the entire driving cycle in the WLTC test. The engine has the following characteristics:

- idling time is 242 s or 15% of the entire test cycle;
- the WLTC involves 6 non-stationary modes during which engine crankshaft speed increases from neutral load or, if the vehicle is equipped with a start-stop system, the engine is shut down and then started;
- instantaneous power momentarily coincides with points in the speed characteristic, which is not typical of the NEDC;
- the portion of the driving cycle when load is limited to 50% of the maximum load and the rotational speed of the crankshaft ranges from 1200 to 3000 rpm can be identified.

Fuel consumption in the WLTC is higher than in the NEDC test, in both older and brand-new vehicles, approximating real-world fuel consumption. In the NEDC, fuel consumption is measured under specific driving conditions,

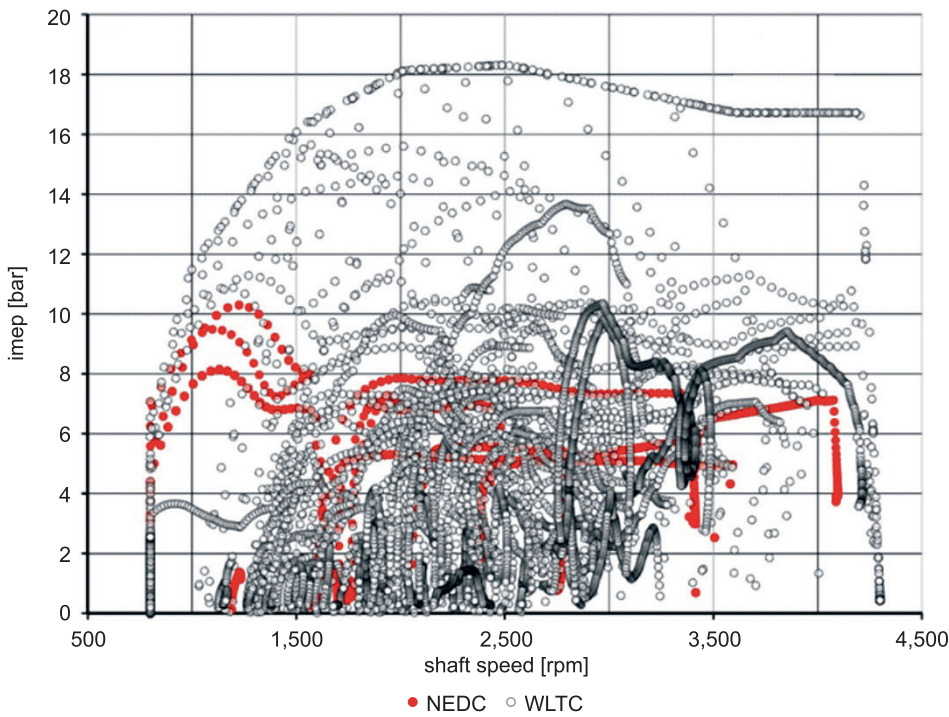


Fig. 2. Indicated mean effective pressure (IMEP) in a light-duty vehicle (GVW 3500 kg) in NEDC and WLTC tests

such as urban and extra-urban driving. The transition from the NEDC to the WLTC started in 2017, and fuel consumption is currently measured in speed intervals. Different testing speeds and maximum speeds are applied to various vehicle classes. Fuel consumption in the NEDC and the WLTC is compared in Tables 1 and 2.

Table 1

Fuel consumption in Toyota Yaris

Toyota Yaris 1.5			
NEDC		WLTC	
Test conditions	fuel consumption [L/100 km]	speed	fuel consumption [L/100 km]
Urban	6.5	low	7.9
Extra-urban	4.3	medium	5.9
Combined cycle	5.1	high	5.2
—	—	very high	6.1
—	—	combined cycle	6.0

Source: own elaboration based on the manufacturer’s specifications.

Table 2

Fuel consumption in Toyota RAV4 SUV			
Toyota RAV4 2.0			
NEDC		WLTC	
Test conditions	fuel consumption [L/100 km]	speed	fuel consumption [L/100 km]
Urban	6.8	low	8.9
Extra-urban	5.4	medium	7.2
Combined cycle	5.9	high	6.3
–	–	very high	7.7
–	–	combined cycle	7.3

Source: own elaboration based on the manufacturer's specifications.

The compared driving cycles produced different results. The WLTC test has steeper accelerations and higher engine load than the NEDC. As a result, fuel consumption better reflects real-world driving conditions. Regardless of the driving cycle, instantaneous engine torque can be expressed as follows:

$$M_e = \frac{\left(m \cdot g \cdot f_r \cdot \cos \alpha + 0.5 \cdot \rho_a \cdot C_x \cdot A \cdot V^2 + m \cdot \delta \cdot \frac{dV}{dt}\right) \cdot r_d}{i_g \cdot i_o \cdot \eta_t} \quad (17)$$

When the change in time is relatively small, it can be assumed that the vehicle moves in linear motion and its acceleration is constant. Instantaneous torque M at any point in the driving cycle can be calculated with formula (17). Depending on speed, instantaneous points in the driving cycle denote the operating region of the powertrain. The relevant information plays a very important role during the development of optimization techniques. Powertrain performance should be maximized at points representing higher loads.

Selection of decision parameters, functional limitations and quality criteria

During optimization, special attention is paid to vehicle dynamics, including acceleration (formula 16) and braking distance (FRIES et al. 2018, GILLESPIE 1992, LI et al. 2020, WALIGÓRSKI, KUCAL 2018). A set of dynamic indicators can be used to establish quality criteria as well as functional limitations in the optimization problem.

OGLIEVE et al. (2017) proposed an effective analytical procedure for calculating fuel consumption based on the NEDC speed profile. The analysis involved

an integrated optimization procedure to minimize fuel consumption and NO_x emissions as objective functions. Optimal gear ratios were determined for 4-, 5- and 6-speed gearboxes as control parameters in the optimization process. In the analysis, the gear shifting strategy should be determined by minimizing one of the declared objective functions. In the best case scenario, fuel consumption is reduced by 7.5% and NO_x emissions are reduced by 6.75% in a 6-speed gear box where the gear shifting strategy is based on minimal fuel consumption for a given engine type. These results indicate that gearbox optimization is an effective and cheap method of reducing fuel consumption and harmful emissions.

The appropriate optimization technique should be applied in the process of vehicle modernization. In the bus presented in Table 3, the gear ratio was modified when a spark-ignition engine was replaced with a diesel engine, as recommended by the manufacturer. Spark-ignition and diesel engines have different characteristics (HEYWOOD 1988), and a vehicle’s gear ratio has to be adapted accordingly. The effects of different gear ratios on fuel economy, emissions and engine dynamics are well known. A multi-criteria optimization technique can be applied to make a trade-off between the above parameters.

Table 3

Technical specification of a light-duty vehicle (LDV)

Specification	RUTA-25d (GRYTSYUK, VRUBLEVSKYI 2018)
Vehicle dimensions [mm]	7000/2050/2730
Axle width [mm]	3745
Tire size	232/65 R16
Gross vehicle weight rating/curb weight [kg]	1900/1600
Acceleration 0-100 km/h [s]	–
Maximum velocity [km/h]	130
Average fuel consumption [l/100 km]	19.5
Maximum output [kW/rpm]	88.3/3200
Rated torque [rpm]	3200
Maximum torque [Nm/rpm]	297/1600-2700

Research methodology for optimizing vehicle design

Vehicle design can be optimized with the use of the following strategies or their combinations (VRUBLEVSKYI, WOJNOWSKI 2019):

– Design of Experiments (DoE) methods (ROSS 1998). These methods facilitate the selection of the optimal solution. However, the DoE approach may

produce unsatisfactory results, in particular when only one criterion is selected. Various sampling methods can be used in the DoE approach, including orthogonal arrays, Sobol sequences (SOBOL, STATNIKOV 2006) and Monte Carlo methods (RUBINSTEIN, KROESE 2008);

– optimization methods. Various optimization methods have been proposed. The selection of the appropriate optimization algorithm is a very important consideration because some optimization methods have been designed for specific purposes, depending on spatial parameters (spatial modality, continuity, linearity, etc.).

The effectiveness of these methods increases when they are applied in combination. For example, the first method can be used to plan the experiment, test the boundary values of the analyzed parameters and establish a set of decision parameters. Ultimately, the appropriate optimization method is used to identify the optimal point. In this case, the search for the optimal solution does not begin from zero or in a random manner. The DoE approach is used at the beginning of the optimization process to determine initial search conditions. The optimization problem described in this study was solved with the use of Simcenter Amesim 2019 software (DABADIE et al. 2017, LE BERR et al. 2012, LI et al. 2020).

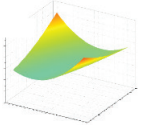
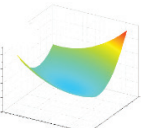
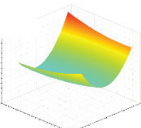
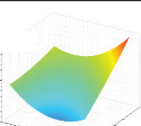
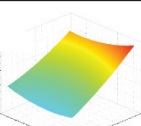
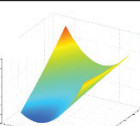
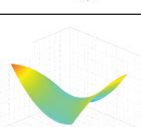
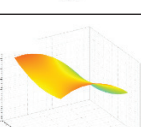
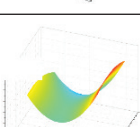
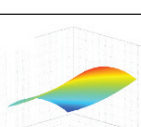
Optimization process

Parameter space analysis in a vehicle with an internal combustion engine

The relationships between gearbox parameters and selected quality criteria, i.e. fuel economy and acceleration, was examined with the use of DoE methods to determine the boundary values of the investigated parameters. The results obtained in this stage of the analysis can be used to narrow down the search space for localizing the global optimum. The relationships presented in Table 4 were determined by calculating sampling points whose input vectors were described with the Monte Carlo method. The values of all parameters had normal distribution. The obtained data were used to analyze the influence of gearbox parameters on selected performance parameters. When the influence of the 2nd and 4th gear ratio on fuel consumption was analyzed, significant differences were noted only for the 4th gear ratio. The system was not sensitive to the 2nd gear ratio. In turn, an analysis of the 3rd and 4th gear ratios revealed that both variables influenced fuel economy.

Sobol sequences were used to derive input parameter vectors for the sampling points, presented in Figure 3. The results of the calculations for each sampling point are localized in the plane of fuel economy criteria – difference in acceleration.

Table 4

Relationship between fuel consumption and gear ratio				
<div><div><div>Y</div><div>X</div></div></div>	1 st gear ratio (i_1)	2 nd gear ratio (i_2)	3 rd gear ratio (i_3)	4 th gear ratio (i_4)
2 nd gear ratio (i_2)				
3 rd gear ratio (i_3)				
4 th gear ratio (i_4)				
5 th gear ratio (i_5)				

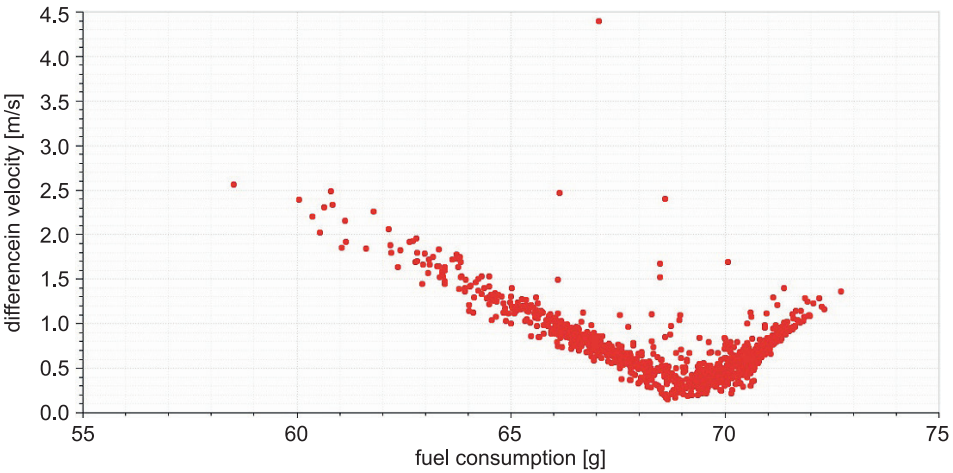


Fig. 3. Sampling points in the space of decision criteria for fuel consumption and the dynamic performance of a vehicle with an internal combustion engine

Trade-off solutions can be identified in the resulting set of solutions, and they are located on the Pareto optimal curve. These points describe the best combination of input parameters, i.e. gear ratios whose implementation contributes to reducing fuel consumption or improving engine dynamics.

Multi-criteria optimization of gearbox parameters

The use of DoE tools in data analysis supports the development of an appropriate set of input parameters in the optimization process the selection of boundary values of decision parameters and quality criteria, as well as the selection of the initial point for localizing the optimum. Two criteria were selected for solving the optimization problem where the Non-Linear Programming by Quadratic Lagrangian (NLPQL) algorithm was used to upgrade the gearbox in a vehicle with an internal combustion engine:

- fuel consumption per 100 km;
- distance traveled during the simulation.

The first criterion was selected on the assumption that the goal of optimization is to reduce fuel consumption during the simulation. The second criterion was adopted to accurately reflect changes in the vehicle's speed based on the speed profile of a given driving cycle. The total distance traveled by the vehicle during the test was compared. The longest distance was indicative of the highest average speed and, consequently, the smallest deviations in linear speed relative to the adopted speed profile.

The results of the optimization procedure for the NEDC and the WLTC are presented in Table 5. When the gearbox was not adapted for use with a diesel engine, fuel consumption was lower by 1 L in the NEDC than in the WLTC. The same difference was noted when the optimization problem was based on fuel consumption only, with a minor decrease in absolute values. The correlation between qualitative variables was maintained when two criteria were applied in the optimization process. Minimal fuel consumption was achieved in the NEDC test (9.97 L/100 km).

Table 5

Fuel consumption [L/100 km] in a vehicle with an internal combustion engine

Cycle	Before optimization	Criterion: fuel consumption	Criteria: fuel consumption and distance
NEDC	10.1885	10.1633	9.97
WLTC	11.6086	11.3575	11.2493

Dynamic engine performance is also highly desirable in vehicles. Therefore, the optimization procedure was based on the time required to achieve a given linear speed. The input parameter was the difference between the final velocity after 45 seconds of acceleration and the test velocity of 25 m/s. The minimum value of the above difference was used to set decision parameters. In this analysis, the decision parameter was the gear ratio. Changes in the vehicle's test velocity, the final velocity and the differences between these values are presented in Figure 4.

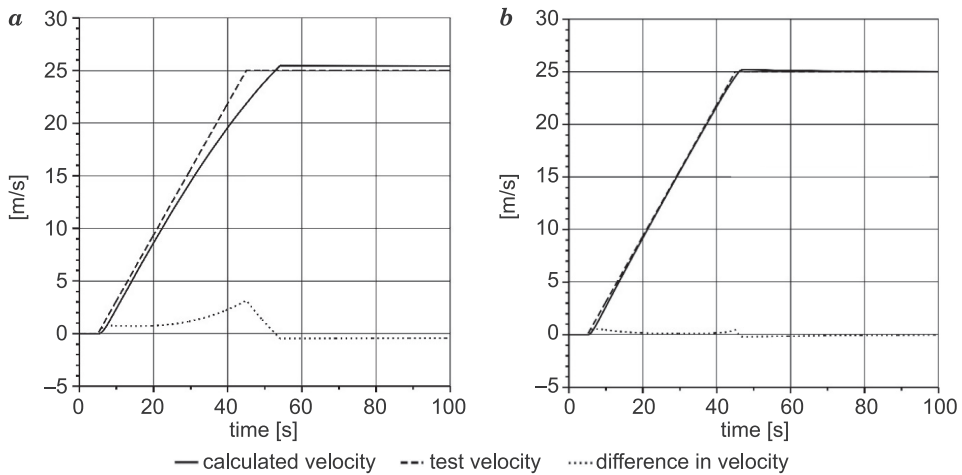


Fig. 4. Changes in velocity during acceleration to 25 m/s over 45 s:
a – before optimization, b – after optimization

The difference in final velocity after optimization was 0.16131 m/s. The gear ratios for each gear were determined at: $i_g = 4.11$; $i_1 = 3.34$; $i_2 = 2.32$; $i_3 = 1.49$; $i_4 = 1.03$; $i_5 = 0.813$.

It should be noted that the NLPQL algorithm is not the only method for solving an optimization problem. When a multi-objective genetic algorithm (GHORBANIAN et al. 2011, MIRJALILI 2019, URBINA CORONADO et al. 2018) was applied to the same decision parameters, a small difference was observed in the values of quality criteria and parameters (Tab. 6). However, an analysis of the results indicates that the NLPQL generated lower values of fuel consumption and CO and NO_x emissions; therefore, it appears to be better suited for solving the presented optimization problem (Tab. 6).

Table 6

Parameter/Criterion	Base	NLPQL	Genetic algorithm
1 st gear ratio (i_1)	2.8	2.8	2.8
2 nd gear ratio (i_2)	1.7	1.7	1.7
3 rd gear ratio (i_3)	1.25	1.25	1.307
4 th gear ratio (i_4)	0.9	1.026	1.00
5 th gear ratio (i_5)	0.813	0.813	0.797
Fuel consumption [g] WLTC	1383	975	985
CO emissions [mg] WLTC	150.6	119.9	119.3
HC emissions [mg] WLTC	17.61	14.45	14.49
NO _x emissions [mg] WLTC	60.67	35.38	36.00

Conclusions

Optimization techniques have to be applied in the process of designing new vehicles and modernizing the existing solutions. Optimization techniques reduce the time and cost of such operations and facilitate the search for trade-off solutions that account for different and often contradictory customer requirements as well as vehicle operating conditions.

This study demonstrated that the effectiveness of the optimization process is determined by the operating conditions of the powertrain. The accuracy of the results can be improved under the conditions prescribed in the WLTC test. A comparison of the optimization results for a vehicle with an internal combustion engine revealed that when the gear box was not adapted for use with a diesel engine, fuel consumption was 1 L lower in the NEDC than the WLTC test. The same difference was noted when the optimization problem was based on only one criterion, i.e. fuel consumption, with a minor decrease in absolute values (10.1633 L/100 km and 11.3575 L/100 km). The correlation between qualitative variables was maintained when two criteria were applied in the optimization process. Minimal fuel consumption was achieved in the NEDC test (9.97 L/100 km).

The criteria for selecting powertrain parameters in a vehicle with an internal combustion engine were fuel economy, engine dynamics, and toxic emissions. When a vehicle with an internal combustion engine was optimized with the involvement of the NLPQL algorithm and the genetic algorithm, only minor differences were noted in the values of quality criteria and parameters. The NLPQL algorithm generated lower values of fuel consumption and CO and NO_x emissions.

The results of this study indicate that optimization techniques can be used to adapt the powertrain to different types of engines by modifying parameters such as the gear ratio. As a result, vehicle parameters can be more accurately tailored to specific user needs and requirements. Gearbox parameters can be accurately adapted to a specific route and terrain by incorporating GPS data and the speed profile in a driving cycle and using real-world road gradients in the simulation model, in particular in the process of modifying the design of municipal buses.

References

- BARLOW T., LATHAM S., MCCRAE I., BOULTER P. 2009. *A reference book of driving cycles for use in the measurement of road vehicle emissions*. TRL Published Project Report, London.
- BERTRAM C., HERZOG H.-G. 2013. *Optimization Method for Drive Train Topology Design and Control of Electric Vehicles*. EVS27 International Battery, Hybrid and Fuel Cell Electric Vehicle Symposium, Barcelona.
- DA COSTA A., ALIX G. 2011. *Enhancing hybrid vehicle performances with limited CO₂ overcost thanks to an innovative strategy*. 2011 EAEC Congress, Valence.
- DABADIE J.C., LE BERR F., SALZGEBER K., PRENNINGER P. 2011. *Evaluation of TEG Potential in Hybrid Electric Vehicle by Simulation*. Vehicle Thermal Management Systems, (10): 15-19.
- DABADIE J.C., SCARRETTA A., FONT G., LE BERR F. 2017. *Automatic Generation of Online Optimal Energy Management Strategies for Hybrid Powertrain Simulation*. SAE Technical Paper 2017-24-0173.
- FRASER N., BLAXILL H., LUMSDEN G., BASSETT M. 2009. *Challenges for increased efficiency through gasoline engine downsizing*. SAE Int. J. Engines, 2(1): 991-1008.
- FRIES M., KRUTTSCHNITT M., LIENKAMP M. 2018. *Operational Strategy of Hybrid Heavy-Duty Trucks by Utilizing a Genetic Algorithm to Optimize the Fuel Economy Multiobjective Criteria*. IEEE Transactions on Industry Applications, 54(4): 3668–3675.
- GHORBANIAN J., AHMADI M., SOLTANI R. 2011. *Design predictive tool and optimization of journal bearing using neural network model and multi-objective genetic algorithm*. Scientia Iranica, Transactions B: Mechanical Engineering, 18: 1095–1105.
- GIKAKOUMIS E.G., ZACHOTIS A.T. 2017. *Investigation of a Diesel-Engine Vehicle Performance and Emissions during the WLTC Driving Cycle - Comparison with the NEDC*. Energies 10: 240.
- GILLESPIE T.D. 1992. *Fundamentals of vehicle dynamics*. Society of Automotive Engineers, Warrendale, PA.
- GRYTSYUK O., VRUBLEVSKIY O. 2018. *Investigations of diesel engine in the road test*. Diagnostyka, 19(2): 89–94.
- HEYWOOD J.B. 1988. *Internal Combustion Engine Fundamentals*. McGraw Hill, New York.
- HUSAIN I., ISLAM M.S. 1999. *Design, Modeling and Simulation of an Electric Vehicle System*. SAE Paper 1999-01-1149.
- KROPIWNICKI J. 2011. *Ocena efektywności energetycznej pojazdów samochodowych z silnikami spalalinowymi*. Monografie, 110.
- LE BERR F., ABDELLI A., POSTARIU D.-M., BENLAMINE R. 2012. *Design and Optimization of Future Hybrid and Electric Propulsion Systems An Advanced Tool Integrated in a Complete Workflow to Study Electric Devices Oil & Gas Science and Technology*. Rev. IFP Energies Nouvelles, 67(4): 547-562.
- LI Y., ZHU B., ZHANG N., PENG H., CHEN Y. 2020. *Parameters optimization of two-speed powertrain of electric vehicle based on genetic algorithm*. Advances in Mechanical Engineering, 12(1).

- MIRJALILI S. 2019. *Genetic algorithm. Evolutionary algorithms and neural networks*. Springer, Cham.
- MITCHKE M. 1977. *Dynamika samochodu*. Wydawnictwa Komunikacji i Łączności, Warszawa.
- OGLIEVE C., MOHAMMADPOUR M., RAHNEJAT H. 2017. *Optimisation of the vehicle transmission and the gear-shifting strategy for the minimum fuel consumption and the minimum nitrogen oxide emissions*. Proceedings of the Institution of Mechanical Engineers, Part D: Journal of Automobile Engineering, 231(7): 883-899.
- Optimize system performance from early design stages. Simcenter Amesim*. Siemens. <https://www.plm.automation.siemens.com/global/en/products/simcenter/simcenter-amesim.html>.
- ORZEŁOWSKI S. 1969. *Budowa podwozi i nadwozi samochodowych*. WSiP, Warszawa.
- PENG M., LIN J., LIU X. 2018. *Optimizing design of powertrain transmission ratio of heavy duty truck*. IFAC-PapersOnLine, 51(31): 892-897.
- ROSS P.J. 1998. *Taguchi Techniques for Quality Engineering*. McGraw-Hill, New York.
- RUBINSTEIN R.Y., KROESE D.P. 2008. *Simulation and the Monte Carlo Method*. Second Edition, J. Wiley & Sons Inc., Hoboken.
- SCHITTKOWSKI K. 1986. *NLPQL: A Fortran subroutine for solving constrained nonlinear programming problems*. Annals of Operations Research, 5(2): 485–500.
- SCHITTKOWSKI K. 2011. *A robust implementation of a sequential quadratic programming algorithm with successive error restoration*. Optimization Letters, 5(2): 283-296.
- SCIARETTA A., DABADIE J., ALBRECHT A. 2008. *Control-Oriented Modeling of Power Split Devices in Combined Hybrid-Electric Vehicles*. SAE Paper 2008-01-1313.
- SHEN W., YU H., HU Y., XI J. 2016. *Optimization of shift schedule for hybrid electric vehicle with automated manual transmission*. Energies, 9(3): 220.
- SKUGOR B., DEUR J. 2014. *Dynamic programming-based optimization of electric vehicle fleet charging*. 2014 IEEE International Electric Vehicle Conference (IEVC), Florence.
- SOBOL I.M., STATNIKOV R.B. 2006. *Choice of optimal parameters in a framework with many criteria*. Drofa, Moskwa.
- URBINA CORONADO P.D., ORTA CASTAÑÓN P., AHUETT-GARZA H. 2018. *Optimization of gear ratio and power distribution for a multimotor powertrain of an electric vehicle*. Engineering Optimization, 50(2): 293–309.
- VERDONCK N., CHASSE A., POGNANT-GROS P., SCIARRETTA A. 2010. *Automated model generation for hybrid vehicles optimization and control*. Oil & Gas Science and Technology – Revue de l'Institut Français du Pétrole, 65(1): 115-132.
- VRUBLEVSKIY O., WOJNOWSKI R. 2019. *Development of a method for finding the optimal solution when upgrading a motorcycle engine*. Technical Sciences, 22(2): 125-149.
- WALIGÓRSKI M., KUCAL K. 2019. *The impact of the full power characteristics of the internal combustion engine and the traction characteristics of the vehicle on its safety in urban traffic*. Transportation Research Procedia, 40: 594–601.



Quarterly peer-reviewed scientific journal

ISSN 1505-4675
e-ISSN 2083-4527

TECHNICAL SCIENCES

Homepage: www.uwm.edu.pl/techsci/



DOI: <https://doi.org/10.31648/ts.6087>

INVESTIGATION OF LOW- AND HIGH-CYCLE FATIGUE IN AL 2024-T4 ALLOY

Sylwester Kłysz

ORCID: 0000-0002-4521-4972

Department of Technical Sciences

University of Warmia and Mazury in Olsztyn

Airworthiness Division

Air Force Institute of Technology in Warsaw

Received 6 November 2020, accepted 5 January 2021, available online 5 January 2021.

Key words: low-cycle fatigue, high-cycle fatigue, 2024 aluminum alloy, Manson-Coffin equation, Morrow equation, S-N curves.

Summary

The article presents the results of low- (LCF) and high-cycle fatigue (HCF) analyses of 2024-T4 aluminum alloy which is used in aircraft construction, mainly for highly loaded structural components, including for plating, fuselage frames and rotor blade girders in helicopters. The alloy is used in structures where a high strength-to-weight ratio and high fatigue resistance are required. However, the alloy is poorly weldable and has low corrosion resistance.

The tests were performed on hourglass and cylindrical samples with parallel and perpendicular orientation relative to the rolling direction. Samples for analysis were obtained from the production line of PZL-130 Orlik TC-II trainer aircraft. The results of the analysis were described by Manson-Coffin and Morrow equations.

Correspondence: Sylwester Kłysz, Katedra Mechaniki i Podstaw Konstrukcji Maszyn, Wydział Nauk Technicznych, Uniwersytet Warmińsko-Mazurski, ul. M. Oczapowskiego 11, 10-719 Olsztyn, e-mail: sylwester_k@uwm.edu.pl

Introduction

Aluminum alloys are widely applied in civilian and military engineering (HEINZ et al. 2000, PETRASEK et al. 2013, *Problemy badań i eksploatacji...* 1993). They are used in the production of the structural components of aircraft, including plating, fuselage frames, stringers and hatches. The EN AW-2024 T4 aluminum alloy is used in highly loaded structural components and plating where a high strength-to-weight ratio and high fatigue resistance are required. However, the alloy is poorly weldable and has low corrosion resistance.

Analyses of the performance of aircraft structures indicate that mechanical strain is the main cause of damage to aviation plating (SIENIAWSKI 2002). Plating is damaged due to the initiation and propagation of cracks, and the material's strength is determined by the number of cycles until destruction within a given range of plastic or total strain values (NOGUEIRA et al. 2020, POLAK 1991). Analyses of materials' behavior under variable loads in a small number of cycles provide valuable information and support the identification of cyclic fatigue mechanisms, localization of strain, cracks and failure of structural components (LI et al. 2019, FENG, QIAN 2018, IGNATOVICH et al. 2013).

Analyses of low-cycle fatigue resistance are also helpful in estimating the service life of structural components. The shape of the hysteresis loop during low-cycle fatigue resistance tests and their stabilized dimensions are determined by the type of material and loading conditions. An extensive analysis of fatigue parameters and changes in the shape of the hysteresis loop under various experimental and operating conditions, and the extent to which changes in the properties of materials subjected to cyclic and variable loading (including overloading) affect fatigue resistance and the shape of the hysteresis loop was presented by (GOSS 1982, KŁYSZ 2000). The results of similar studies are found in the literature – however, in order to compare them with each other and apply them to specific analyzes, it is always necessary to take into account the correct composition, mechanical and temperature processing condition of the tested material – which is not always clearly documented. These tests were performed for the purpose of introducing own material characteristics to the FEM strength analyzes of elements made of materials taken directly from the production line of the PZL-130 Orlik TC-II aircraft.

The aim of this study was to describe low- and high-cycle fatigue of hourglass and cylindrical samples of 2024-T4 alloy with the use of Manson-Coffin and Morrow equations. The alloy's fatigue resistance was evaluated in samples with parallel and perpendicular orientation relative to the sheet rolling direction. The results were analyzed by calculating the parameters of Manson-Coffin and Morrow equations as well as the equations presented by the U.S. Department of Transportation of the Federal Aviation Administration (DOT/FAA/AR-MMPDS-01... 2003).

Materials and Methods

The experiment involved hourglass and cylindrical samples with a diameter of $\varnothing 6.5$ mm (Fig. 1). The samples were obtained from the production line of PZL-130 Orlik TC-II trainer aircraft in the following configuration:

- parallel to the rolling direction, (longitudinal samples, T-L orientation),
- perpendicular to the rolling direction, (transverse samples, L-T orientation).

The chemical composition of 2024-T4 alloy based on standard PN-EN 573-3 is presented in Table 1. The mechanical properties of the analyzed alloy are presented in Table 2 according to Standard PN-EN 485-2, in Table 3 according to the specifications of ASM Aerospace Specification Metals Inc., and in Tables 4 and 5 according to MIL-HDBK-5J specifications.

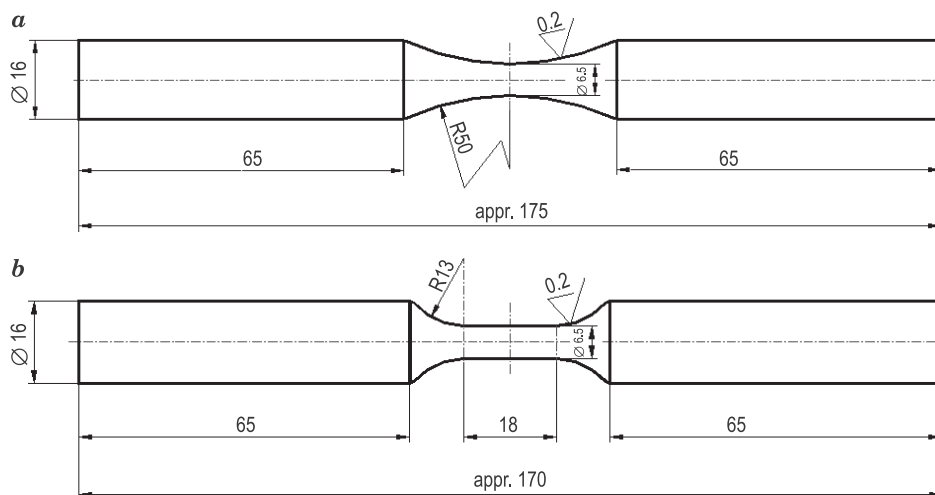


Fig. 1. Shape and dimensions of samples for low- (a) and high-cycle (b) fatigue tests

Table 1

Chemical composition [%] of EN AW-2024 T4 alloy to Standard PN-EN 573-3: 2009

Si	Fe	Cu	Mn	Mg	Cr	Zn	Ti	Other	Al
0.50	0.50	3.8-4.9	0.30-0.9	1.2-1.8	0.10	0.25	0.15	0.15	other

Source: PN-EN 573-3: *Aluminium i stopy aluminium – Skład chemiczny i rodzaje wyrobów przerobionych plastycznie. Część 3: Skład chemiczny i rodzaje wyrobów* (2009).

Table 2

Mechanical properties of EN AW-2024 T4 alloy acc. to Standard PN-EN 485-2: 2009

R_m [MPa]	R_e [MPa]	$A_{50\text{ mm}}$ [%]	HBW
min. 425	min. 275	min. 14	120

Source: PN-EN 485-2: *Aluminium i stopy aluminium – Blachy, taśmy i płyty. Część 2: Własności mechaniczne* (2009).

Table 3

Mechanical properties of 2024 T4 and 2024 T351 alloys acc. to ASM

R_m^* [MPa]	R_e^* [MPa]	A^* [%]	E^* [GPa]	ν	K_{1C} [MPa√m]	Z^* [MPa]	HB*
2024 T4 and 2024 T351							
469	324	19 (Ø = 12.5 mm) 20 (<i>t</i> = 1.6 mm)	73.1	0.33	26 (S-L orientation)	138	(500,000,000 cycles; RR Moore)
					32 (T-L orientation)		
					37 (L-T orientation)		
2024 T3**							
483	345	18 (<i>t</i> = 1.6 mm)	73.1	0.33	–	138 (500,000,000 cycles; RR Moore)	120

* according to the ASM website, these data were provided by Aluminum Association Inc. and are not for design;

** according to the ASM website, these data were provided by Alcoa and are not for design.

Source: ASM Aerospace Specification Metals Inc. <http://asm.matweb.com>.

Table 4

Mechanical properties of 2024 T4 alloy (rolled bars) acc. to MIL-HDBK-5J

$R_{m,\text{min}}$ [MPa]	$R_{e,\text{min}}$ [MPa]	A_{min} [%]	E [GPa]	ν
427 (L orientation) ¹ 420 (L-T orientation) ¹	310 (L orientation) ¹	15 ³	72.4 ⁶ 73.8 ⁷	0.33
	310 (L-T orientation) ¹	12 ⁴		
	290 (L orientation) ²	8 ⁵		
	290 (L-T orientation) ²			

Note: according to (SIENIAWSKI 2002), sample T4 is outdated and should not be used in newly designed structures:

¹ for rolled bars 3,175-25, 4 mm,

² for rolled bars 12,7-25,4 mm,

³ for sheets and plates with a thickness of 0.53-6.32 mm, L-T orientation,

⁴ for sheets and plates with a thickness of 6.35-12.675 mm, L-T orientation,

⁵ for sheets and plates with a thickness of 12.7-25.4 mm, L-T orientation,

⁶ for sheets and plates with a thickness of 0.254-6.32 mm,

⁷ for sheets and plates with a thickness of $\geq 6.35\text{ mm}$.

Source: MIL-HDBK-5J (2003).

Table 5

Mechanical properties of 2024 T3 alloy (sheets thickness of 0.25÷3.25) acc. to MIL-HDBK-5J

$R_{m, \min}$ [MPa]	$R_{e, \min}$ [MPa]	A_{\min} [%]	E [GPa]	ν
448 (L orientation)	331 (L orientation)	12	72.4	0.33
441 (L-T orientation)	296 (L-T orientation)	(L-T orientation)	(L-T orientation)	

Note: the presented values of R_m , R_e , A_{\min} , E and ν can be used for designing structural components of military aircraft, naval vessels and FAA aircraft.

Source: MIL-HDBK-5J (2003).

The low-cycle fatigue life of the examined samples was analyzed by determining fatigue durability (N_f) as a function of transverse strain ($\varepsilon_{\text{trans}}$) amplitude in the MTS 370.10 load frame with the MTS 632.18-F20 (measurement range 50 kN), cross-sectional strain extensometer (measurement range $\pm 2\%$). Loading frequency ranged from 0.05 Hz to 1 Hz.

The high-cycle fatigue of the samples was analyzed by determining fatigue durability (N_f) as a function of stress (σ_a) amplitude. The tests were carried out at a load frequency ranging from 15 Hz to 45 Hz.

Sampling rate 200 points/cycle. The tests were performed at room temperature, in the accredited Materials Testing Laboratory of the Air Force Institute of Technology. The test stands are presented in Figure 2.



Fig. 2. Samples analyzed in MTS 810.23 load frame with a cross-sectional strain extensometer

Analysis of low-cycle fatigue

The initial and middle (corresponding to approximately half the number of load cycles to failure) hysteresis loops were determined in each test, and the initial and stabilized values (accounting for the strengthening of the material under cyclic loading) of test parameters were determined for further analyses. Examples of stabilized hysteresis loops for transverse and longitudinal samples are presented in Figure 3.

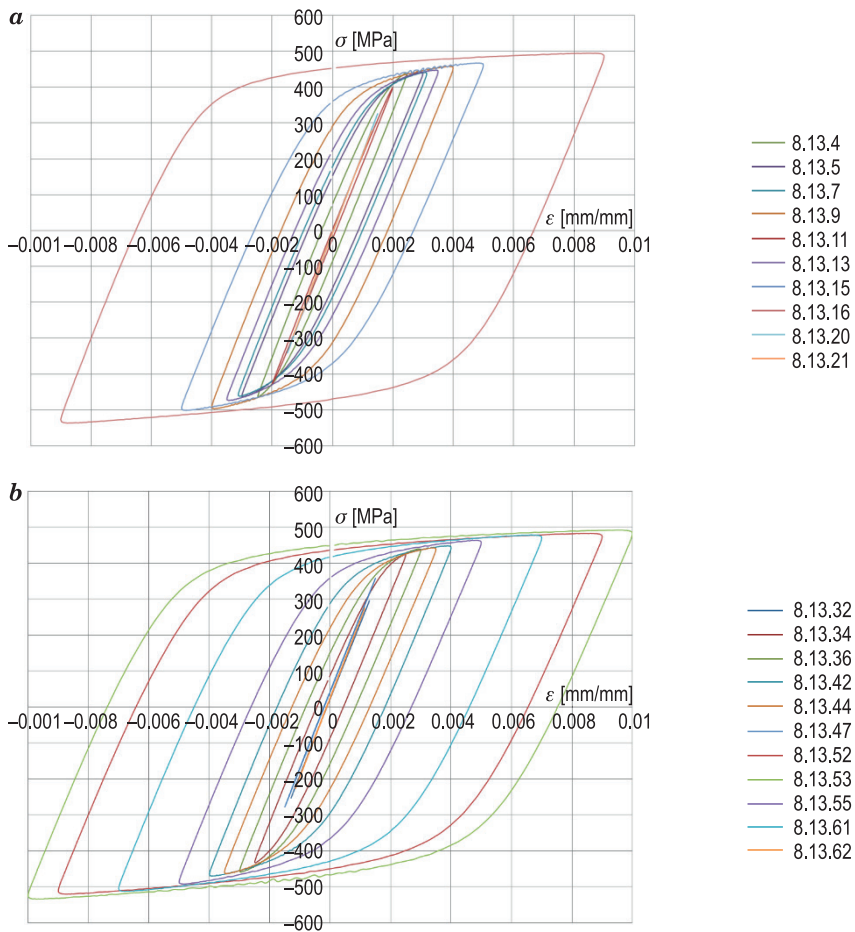


Fig. 3. Hysteresis loops: *a* – transverse samples, *b* – longitudinal samples

The Manson-Coffin relationship and coefficients were determined with the use of the following equation:

$$\frac{\Delta \varepsilon}{2} = \frac{\Delta \varepsilon_e}{2} + \frac{\Delta \varepsilon_{pl}}{2} = \varepsilon_f (2N_f)^a + \sigma_f (2N_f)^b \quad (1)$$

where:

$\varepsilon_{trans} = f(N_f)$, for data corresponding to the first and middle hysteresis loops (Fig. 4 and Fig. 5),

$2N_T$ and ε_T – coordinates of the point of intersection of lines $\varepsilon_e - 2N_f$ and $\varepsilon_{pl} - 2N_f$

The least squares method was used for individual components of deformation (elastic and plastic). The applied transverse strain $\varepsilon_{\text{trans}}$ was converted to longitudinal strain $\varepsilon_{\text{long}}$ with the use of the following formulas:

$$\varepsilon = \varepsilon_e + \varepsilon_{\text{pl}}, \quad \varepsilon_{\text{long},e} = \frac{1}{\nu} \varepsilon_{\text{trans},e}, \quad \varepsilon_{\text{trans},\text{pl}} = \frac{1}{0.5} \varepsilon_{\text{trans},\text{pl}} \quad (2)$$

where ν is Poisson's ratio for stresses within the elastic range.

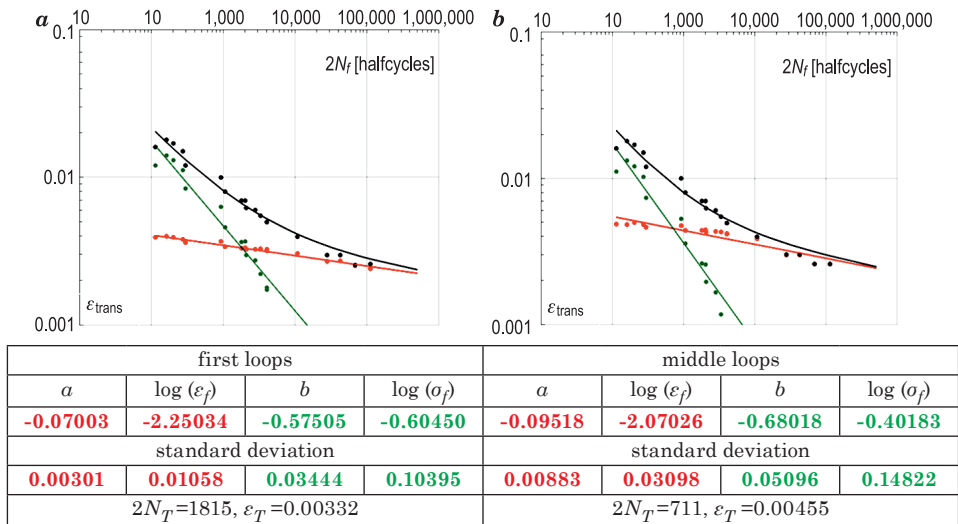


Fig. 4. Manson-Coffin curves for low-cycle fatigue data in the first (a) and middle (b) hysteresis loops in each test (transverse strain) – transverse samples

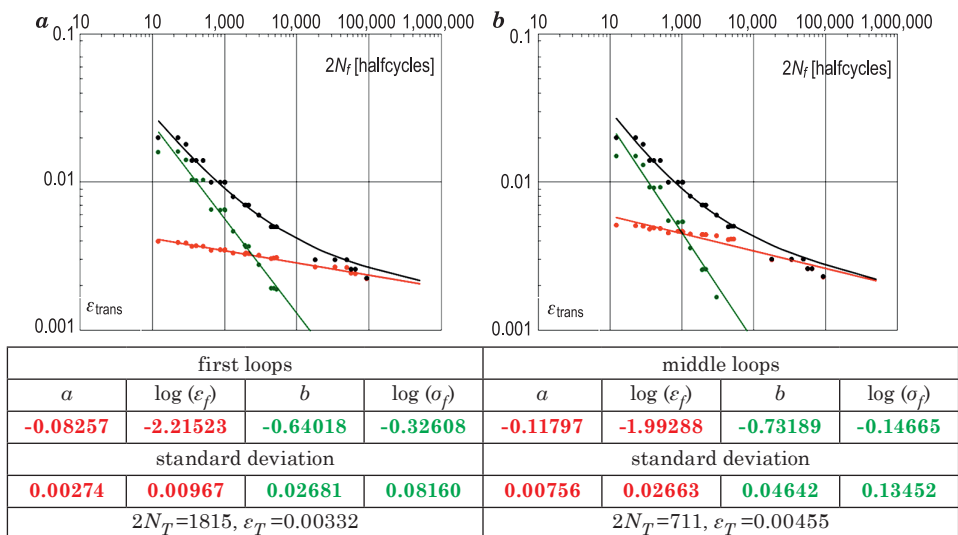


Fig. 5. Manson-Coffin curves for low-cycle fatigue data in the first (a) and middle (b) hysteresis loops in each test (transverse strain) – longitudinal samples

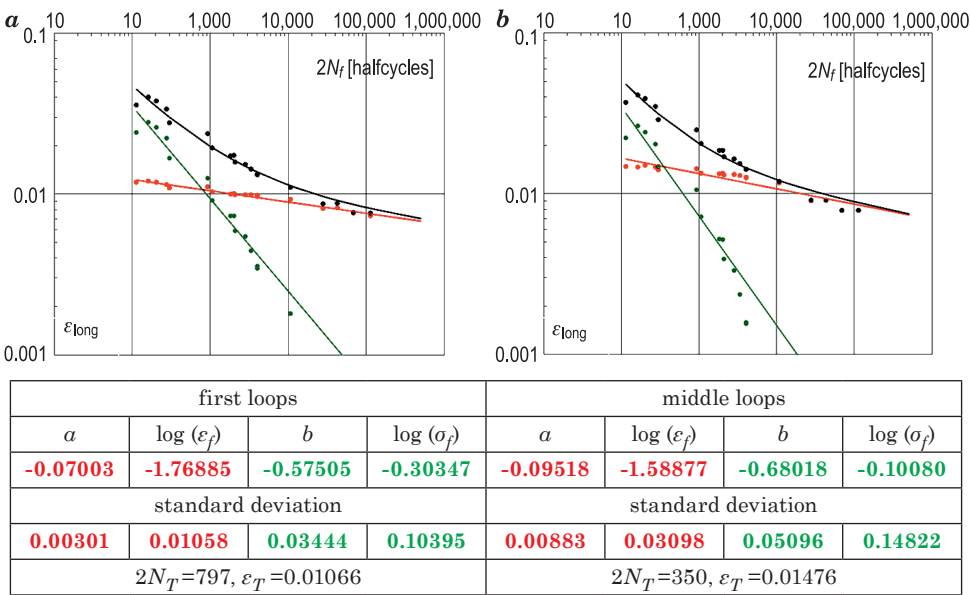


Fig. 6. Manson-Coffin curves for low-cycle fatigue data in the first (a) and middle (b) hysteresis loops in each test (longitudinal strain) – transverse samples

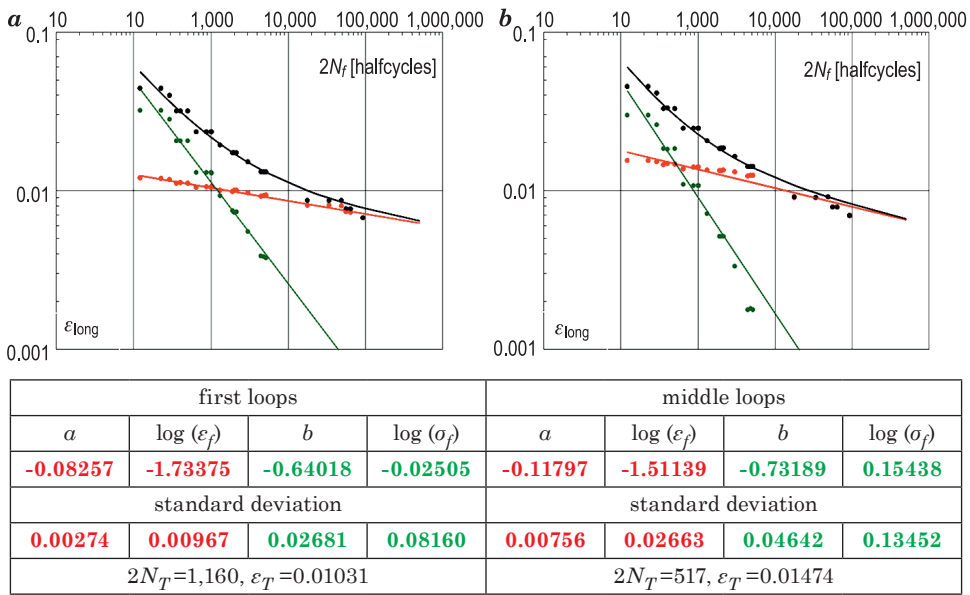
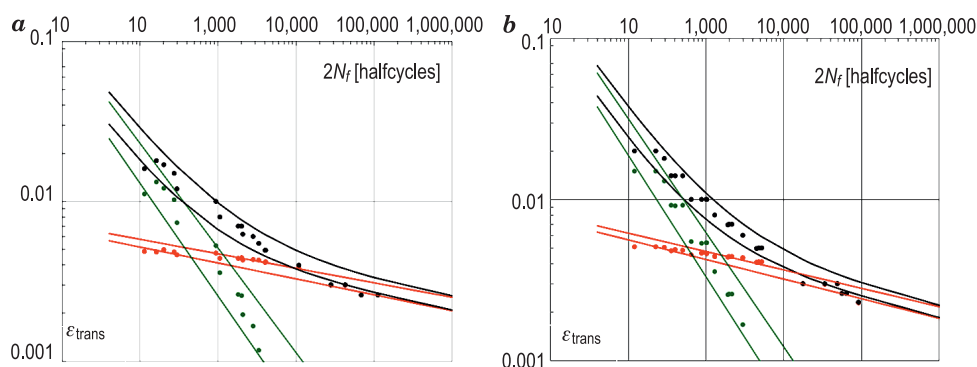
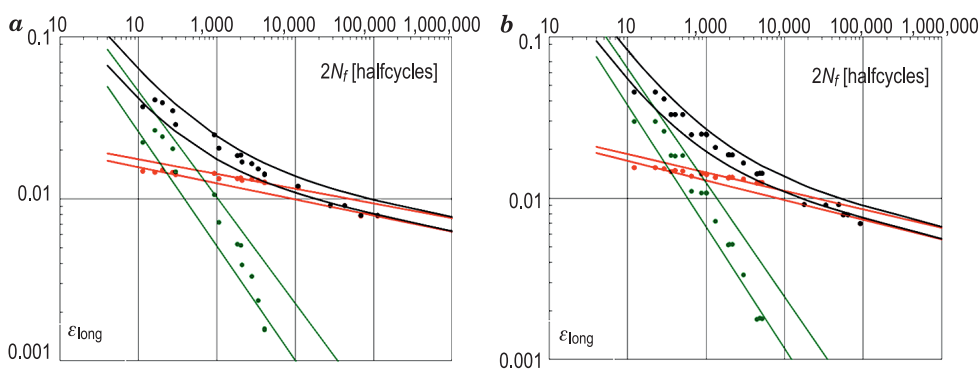


Fig. 7. Manson-Coffin curves for low-cycle fatigue data in the first (a) and middle (b) hysteresis loops in each test (longitudinal strain) – longitudinal samples



transverse samples				longitudinal samples			
a	$\log(\varepsilon_f)$	b	$\log(\sigma_f)$	a	$\log(\varepsilon_f)$	b	$\log(\sigma_f)$
upper limit				upper limit			
-0.09076	-2.05477	-0.65470	-0.32772	-0.11419	-1.97956	-0.70868	-0.07939
lower limit				lower limit			
-0.09959	-2.08575	-0.70567	-0.47593	-0.12175	-2.00620	-0.75510	-0.21391

Fig. 8. Manson-Coffin curves – fatigue limits in low-cycle fatigue curves for middle hysteresis loops in each test – transverse strain



transverse samples				longitudinal samples			
a	$\log(\varepsilon_f)$	b	$\log(\sigma_f)$	a	$\log(\varepsilon_f)$	b	$\log(\sigma_f)$
upper limit				upper limit			
-0.09076	-1.57328	-0.65470	-0.02669	-0.11419	-1.49807	-0.70868	0.22164
lower limit				lower limit			
-0.09959	-1.60427	-0.70567	-0.17490	-0.12175	-1.52471	-0.75510	0.08712

Fig. 9. Manson-Coffin curves – fatigue limits in low-cycle fatigue curves for middle hysteresis loops in each test – longitudinal strain

Manson-Coffin relationships and coefficients at $\varepsilon_{\text{long}} = f(N_f)$ were determined for the data corresponding to the first and middle hysteresis loops (Fig. 6 and Fig. 7).

Manson-Coffin relationships and coefficients at coordinates $\varepsilon_{\text{trans}} = f(N_f)$ and $\varepsilon_{\text{long}} = f(N_f)$ were determined for the data corresponding to the middle hysteresis loops as the lower and upper limits of fatigue relative to the relationships shown in Figures 4b, 5b, 6b and 7b. The width of the fatigue limit was determined based on the standard deviation of each coefficient in the Manson-Coffin equation (Fig. 8 and Fig. 9).

Analysis of high-cycle fatigue

The high-cycle fatigue of the examined samples was analyzed for stress curves $\sigma = f(N)$:

– The equations and the coefficients were determined with the use of formula (3) (KŁYSZ et al. 2010):

$$\sigma_a = \text{Be} \left(\frac{1}{\left(\frac{2N_f}{E} \right)^D + C} \right)$$

(3)

in two variants: $\sigma = f(2N_f)$ (as a function of the number of half-cycles) and $\sigma = f(N_f)$ (as a function on the number of cycles). The resulting curves and coefficients are presented in Figure 10.

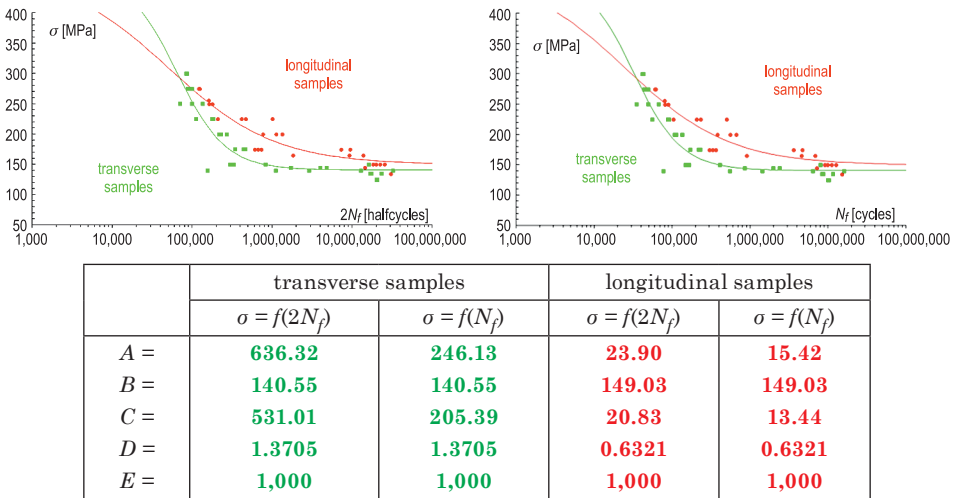


Fig. 10. Stress $\sigma = f(N)$ calculated with formula (3) for transverse and longitudinal samples of 2024 T4 alloy

– The equation and the coefficients were determined with the use of formula (4) (DOT/FAA/AR-MMPDS-01 2003):

$$\log(N_f) = A + B \log(S_{eq} - C) \quad (4)$$

$$S_{eq} = S_{max}(1 - R)^D$$

The resulting curves and coefficients are presented in Figure 11.

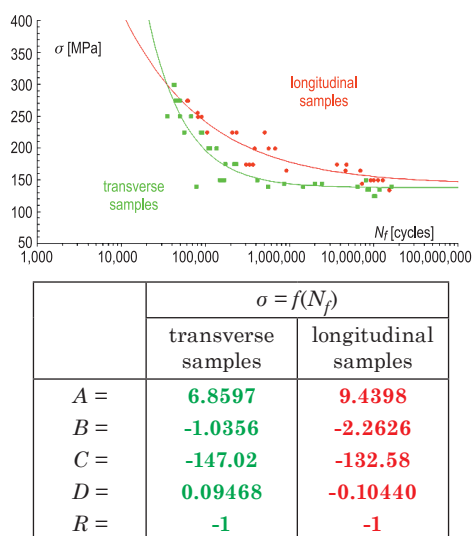


Fig. 11. Stress $\sigma = f(N_f)$ calculated with formula (4) for transverse and longitudinal samples of 2024 T4 alloy

The curves described by equations (3) and (4) are compared in Figure 12.

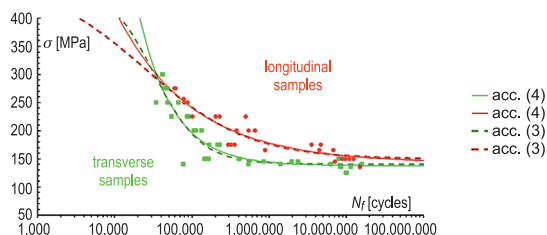


Fig. 12. Stress $\sigma = f(N_f)$ calculated with equations (3) and (4) for transverse and longitudinal samples of 2024 T4 alloy

Conclusions

A comparison of Manson-Coffin curves in low-cycle fatigue analyses demonstrates that transverse samples are characterized by somewhat longer low-cycle fatigue than longitudinal samples. The range of elastic strain components increases, and the range of plastic strain components decreases (coefficients ε_f and σ_f respectively) during fatigue tests, which indicates that the rigidity of the examined samples decreases during tests. These changes are estimated at 10%.

The slope of Manson-Coffin curves (exponents a and b) increases with the cyclic stabilization of test conditions, which decreases the number of cycles and increases deformation at the point of curve intersection. These changes are estimated at 25-40%.

The above changes in Manson-Coffin coefficients occur regardless of sample type (longitudinal/transverse) or type of strain ($\varepsilon_{\text{trans}}/\varepsilon_{\text{long}}$); therefore, stabilized hysteresis loops can be predicted based on the first hysteresis loops. Since only two points are required to plot a line, Manson-Coffin curves can be correctly plotted when the low-cycle fatigue analysis is limited to only two extreme (or randomly selected) loads. However, this procedure requires further experimental verification and analysis.

The stabilized hysteresis loops are characterized by greater divergence than initial hysteresis loops. The above also leads to a greater scatter of fatigue limit values in the tested samples.

At $\varepsilon_{\text{trans}} = f(2N_f)$, the Manson-Coffin equation can be written in a conservative form based on the averaged values of the coefficients for the upper and lower fatigue limits:

$$\frac{\Delta\varepsilon}{2} = 0.0100 \cdot (2N_f)^{-0.1066} + 0.6620(2N_f)^{-0.7060} \quad (5)$$

and the optimistic version of the equation can be expressed by:

$$\frac{\Delta\varepsilon}{2} = 0.0085 \cdot (2N_f)^{-0.1066} + 0.3951(2N_f)^{-0.7060} \quad (6)$$

A comparison of Morrow curves for high-cycle analyses indicates that longitudinal samples are characterized by significantly longer high-cycle fatigue than transverse samples.

Stress curves $\sigma = f(N)$ described with equations (3) and (4) can be regarded as equivalent within the range of the experimental data. The relationship presented in formula (3) assumes a more realistic course when fatigue limits are lower or higher than those determined in this experiment.

References

- ASM Aerospace Specification Metals Inc. <http://asm.matweb.com>.
- DOT/FAA/AR-MMPDS-01. *Metallic Materials Properties*. 2003. Development and Standardization (MMPDS), U.S. Department of Transportation Federal Aviation Administration.
- FENG L, QIAN X. 2018. *Low cycle fatigue test and enhanced lifetime estimation of high strength steel S550 under different strain ratios*. Marine Structures, 61: 343–360.
- GOSS C. 1982. *Doświadczalna i teoretyczna analiza własności stali o podwyższonej wytrzymałości w zakresie małej liczby cykli obciążenia*. Biuletyn WAT, 11.
- HEINZ A., HASZLER A., KEIDEL C., MOLDENHAUER S., BENEDICTUS R., MILLER W. 2000. *Recent development in aluminium alloys for aerospace applications*. Material Sciences and Engineering A, 280: 102–107.
- IGNATOVICH S.R., MENOU A., KARUSKEVICH M.V., MARUSCHAK P.O. 2013. *Fatigue damage and sensor development for aircraft structural health monitoring*. Theoretical and Applied Fracture Mechanics, 65: 23–27.
- KŁYSZ S. 2000. *Wpływ przeciążeń i sekwencji obciążeń na własności niskocyklowe stali 18G2A i St3SY*. Zagadnienia Eksploatacji Maszyn, 4(124): 139–154.
- KŁYSZ S., LISIECKI J., BĄKOWSKI T. 2010. *Modyfikacja równania do opisu krzywych Wöhlera*. Prace Naukowe ITWL, 27: 93–97.
- LI Y., RETRAINT D., XUE H., GAO T., SUN Z. 2019. *Fatigue properties and cracking mechanisms of a 7075 aluminum alloy under axial and torsional loadings*. Procedia Structural Integrity, 19: 637–644.
- MIL-HDBK-5J. *Department of Defense Handbook-Metallic Materials and Elements for Aerospace Vehicle Structures*. 2003.
- NOGUEIRA F., CUNHA J., MATEUS A., MALÇA C., COSTA J.D., BRANCO R. 2020. *Cyclic plastic behaviour of 7075 aluminium alloy*. 1st Virtual Conference on Structural Integrity – VCSI.1 Procedia Structural Integrity, 25: 438–444.
- PETRASEK M., IGNATOVICH S., KARUSKEVICH M., MASLAK T. 2013. *Surface of metal as an indicator of fatigue damage*. Advances in Military Technology, 8(2): 83–91.
- PN-EN 485-2: *Aluminium i stopy aluminium – Blachy, taśmy i płyty*. Część 2: Własności mechaniczne. 2009.
- PN-EN 573-3: *Aluminium i stopy aluminium – Skład chemiczny i rodzaje wyrobów przerobionych plastycznie*. Część 3: Skład chemiczny i rodzaje wyrobów. 2009.
- POLAK J. 1991. *Cyclic plasticity and low cycle fatigue life of metals*. Materials Science Monographs, 63. *Problemy badań i eksploatacji techniki lotniczej*. T.2. Eds. J. Lewitowicz, J. Borgoń, W. Ząbkowicz. Wyd. ITWL, Warszawa.
- SIENIAWSKI J. 2002. *Rozwój metod projektowania i oceny mikrostruktury i właściwości materiałów konstrukcyjnych dla techniki lotniczej*. In: *Postępy nauki o materiałach i inżynierii materiałowej*. Ed. M. Hetmańczyk. Wydawnictwa Politechniki Śląskiej, Katowice.



Quarterly peer-reviewed scientific journal

ISSN 1505-4675
e-ISSN 2083-4527

TECHNICAL SCIENCES

Homepage: www.uwm.edu.pl/techsci/



DOI: <https://doi.org/10.31648/ts.6116>

COMPARISON OF PLOUGHING VS. PLOUGHLESS CULTIVATION IN TERMS OF ENERGY EXPENDITURE AND TREATMENT QUALITY

Piotr Szczyglak

ORCID: 0000-0002-8218-1540

Department of Vehicle and Machinery Construction and Operation
University of Warmia and Mazury in Olsztyn

Received 11 November 2020, accepted 28 December 2020, available online 5 January 2021.

Key words: ploughless cultivation, aggregated tillage unit, innovative machine.

Abstract

The article discusses the basic soil cultivation technologies and analyses the effectiveness of ploughless cultivation machines manufactured in Poland. The study also describes the design of a prototype of an innovative MultiCat 6HD aggregated tillage unit and presents the research methodology for examining the aggregated unit and machines for traditional plough tillage. The following parameters were determined: fuel consumption, theoretical and effective field capacity, depth at which plant residues are incorporated into the soil, and the indicator of crop residue embedding. The conducted analyses revealed that ploughless cultivation required approximately 30% less fuel than traditional plough tillage. Plant material was also more favourably distributed within the soil profile and crop residues were nearly identically embedded as in plough tillage. The study demonstrated that ploughless cultivation involving the MultiCat 6HD aggregated unit can increase the competitiveness of agricultural farms.

Introduction

One of the goals of agricultural policy is to improve the competitiveness of agricultural farms. To achieve this goal, agricultural farms and enterprises can rely on European funds for innovative projects (GORYŃSKA-GOLDMANN, WOJCIESZAK 2017). Most farms improve their competitive edge by introducing innovative production technologies and dedicated machinery. The introduced technologies improve a farm's economic performance and quality indicators by decreasing fuel consumption and energy inputs, improving fertiliser mixing with soil and the incorporation of crop residues.

Tillage, namely a series of agronomic treatments which aim to provide crops with optimal sowing and growth conditions, is one of the most common agricultural operations. Classical tillage involves ploughing and soil preparation before sowing, usually with an aggregated tillage unit (PRZYBYŁ et al. 2009). These treatments may be preceded by post-harvest tillage (PIEKARCZYK 2006). The ploughing treatment itself requires considerable energy inputs in the range of 115.4 to 198.1 kJ·m⁻², and pre-sowing tillage consumes 57.6 to 75.3 kJ·m⁻² of energy (SĘK, PRZYBYŁ 1993). During ploughing, approximately 150 Mg of soil is lifted and inverted per each centimetre of working depth per 10,000 m², and fuel consumption accounts for 30-60% of fuel inputs in the entire crop production process (KUŚ 2007).

Changes in the soil cultivation technology should reduce energy inputs and improve efficiency without deteriorating growth conditions (GOLKA, PTASZYŃSKI 2014). The following alternative tillage technologies have been promoted for many years (SMAGACZ 2013):

- simplified tillage (which reduces the number of cultivation or decreases cultivation depth);
- conservation tillage (comprising ploughless cultivation and zero tillage).

Ploughless cultivation and zero tillage systems considerably reduce the energy inputs in the cultivation process. In ploughless cultivation, ploughing is replaced by treatments that loosen the soil without inverting it (FISZER et al. 2006). In turn, zero tillage eliminates separate soil-loosening treatments from the cultivation process (SMAGACZ 2013).

Conservation tillage is most widely applied in South America (60% of land under cultivation). In Europe, conservation tillage covers only 2.8% of agricultural land, and this technology is likely to attract growing interest in the years to come (KASSAM et al. 2015).

Zero tillage requires significantly more spending on plant protection products which have an adverse effect on the environment. Therefore, ploughless cultivation is a more desirable solution which offers the following benefits (GOLKA, PTASZYŃSKI 2014, SMAGACZ 2013):

- smaller loss of soil organic matter,
- increased organic carbon sequestration in the soil,
- enhanced soil infiltration,
- smaller loss of unproductive water from soil,
- reduced runoff and leaching of fertiliser components,
- improved livestock housing conditions (KOSEWSKA 2018, TOPA 2020),
- lower cultivation costs and greenhouse gas emissions.

The disadvantages of this technology include the risk of weed development and higher incidence of plant diseases and pests (JAKUBOWSKA, MAJCHRZAK 2013). The risk is particularly high when the design of aggregated tillage units does not ensure sufficiently deep incorporation of crop residues covering the soil surface.

The Department of Vehicle and Machinery Construction and Operation of the University of Warmia and Mazury in Olsztyn analysed agricultural machines manufactured by 75 domestic companies (as at 2016) to select aggregated units that are best suited for ploughless cultivation. The analysis revealed that ploughless cultivation units with the following design characteristics are not manufactured in Poland:

- a disc section with hydraulic overload protection devices;
- teeth for deep loosening with a hydraulic overload protection device (hydraulic protection systems facilitate the rapid return of an operating part to its nominal working position, which improves soil cultivation quality);
- a three-point suspension system with positioning control (working segments that require the additional weight of the unit's frame can be freely ganged);
- a disc section preceding the tooth section;
- soil loosening to a depth of 0.4 m with the use of machines ganged with high-power tractors (over 300 kW).

The MultiCat 6HD prototype of an aggregated unit for ploughless cultivation was designed and developed by a domestic manufacturer based on the above requirements. The machine is an innovative solution on the domestic market.

The MultiCat 6HD aggregated tillage unit has a working width of 6 m, and it is designed for ganging with tractors with the minimum engine power of 310 kW (Fig. 1). The unit was designed as a trailing implement, and it features four working sections. The first two sections are permanently attached to the load bearing frame supported with rubber tyre ground wheels. A coupling system is attached to the front part of the frame, and a three-point suspension system for aggregating sections 3 and 4 with an independent load bearing frame is attached to the rear part of the frame. MultiCat 6HD is multi-functional tillage unit. The four sections prepare soil for sowing without plough tillage. The first section comprises two rows of toothed discs with a diameter of 0.68 m. The discs are grouped into four segments, with two segments per row. Each segment has a shared, self-aligning beam to which seven discs are attached with brackets.

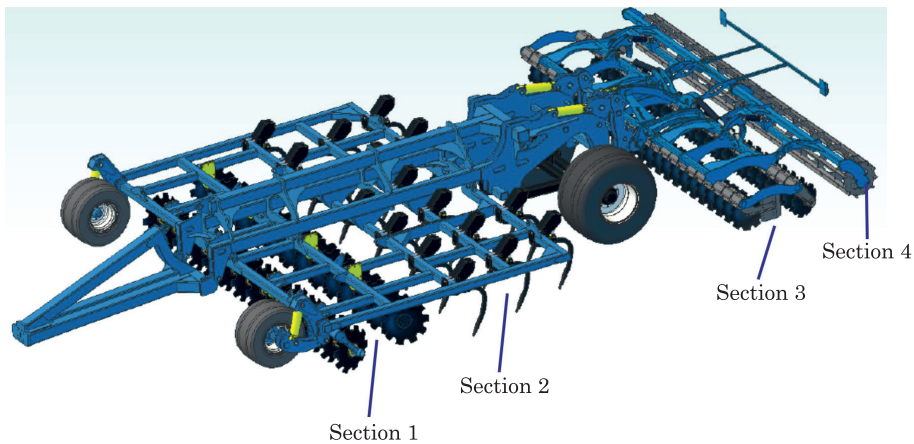


Fig. 1. A view of the MultiCat 6HD aggregated tillage unit in a working position

This type of disc assembly produces a constant rake angle of 17° . Each of the four segments is equipped with a hydraulic overload protection device. The first section cuts the field surface and crop residues, incorporates and mixes crop residues with soil, and cuts roots. The first section has a maximum working depth of 0.2 m, and it can also loosen the soil to decrease the working resistance of the second section and minimise clogging. The second section comprises four rows of teeth for deep soil loosening. This arrangement effectively prevents crop residues from clogging the second section (teeth have a spacing of 0.365 m). Each tooth is equipped with a hydraulic overload protection device. The second section loosens subsoil and combines it with the top soil layer. It has a maximum working depth of 0.4 m.

The third section comprises two rows of toothed discs with a diameter of 0.51 m. A total of 48 discs are attached to two rigid beams that are divided into two segments with supports and brackets. This type of disc assembly produces a constant rake angle of 17° . Each disc has an independent rubber shock absorber mounted in the support. The third section cuts crop residues, incorporates them into the soil and levels out the deformations in the surface of the field caused by the second section. The third section has a maximum working depth of 0.15 m. The spacing between discs is 0.25 m to prevent clogging with plant material.

The fourth section features a string roller with a diameter of 0.61 m, divided into two segments. The fourth section lightly compacts the soil and crushes lumps of soil. The string roller forms a loose and pulverised soil layer underlain by a lightly compacted soil layer.

The aim of this study was to compare the energy and quality indicators calculated based the performance of the MultiCat 6HD aggregated tillage unit prototype (ploughless cultivation) and a conventional plough and disc harrow (traditional cultivation).

Materials and Methods

A passive experiment was conducted in 2016. The parameters of the work process were set by the owner of an agricultural farm owner where the experiment was conducted. The aim of the study was to calculate energy and quality indicators based on empirical data (changes in cultivation technology without the involvement of external agents). The experiment was conducted on a hilly plot with an estimated area of $20 \cdot 10^4 \text{ m}^2$ and varied soil structure. Spring wheat had been combine-harvested three weeks before the experiment. The harvested wheat straw was cut, pulverised and evenly distributed across the field. The plot was moderately infested with weeds, some areas were periodically water logged, and the plot featured tree and shrub clusters. The weather during the field experiment was sunny and partly cloudy, without any rainfall, and daytime temperature ranged from 20°C to 25°C . Ploughless cultivation was performed by the MultiCat 6HD tillage unit ganged with a New Holland T9.670 tractor with twinned wheels (Fig. 2).



Fig. 2. A view of the MultiCat 6HD tillage unit ganged with a New Holland T9.670 tractor

The second analysed agricultural treatment was plough tillage which was performed in two stages. In the first stage, soil was ploughed by a tractor-pulled aggregated unit comprising the New Holland T8050 tractor and the Rabe Werk Marabu-Avant 180C plough. In the second stage, soil was prepared for spring sowing using a disc harrow ganged with the New Holland T8050 tractor. The disc harrow was disconnected from the MultiCat 6HD unit for ploughless cultivation (sections 3 and 4).

The percentage of crop residues that were embedded in the surface layer of soil was analysed in three locations in each experimental plot. Crop residues were collected from the frame with an area of 1 m^2 , and were weighed.

This operation was carried out twice, before and after tillage. The percentage of crop residues embedded in the surface layer of soil was determined by calculating the arithmetic mean of three measurements. The indicator of residue surface embedding R_r , expressed in %, was calculated using the following formula:

$$R_r = \frac{(m_p - m_k)}{m_p} \cdot 100 [\%] \quad (1)$$

where:

m_p – weight of plant residues collected from an area of 1 m² before cultivation [kg],

m_k – weight of plant residues collected from an area of 1 m² after cultivation [kg].

The collected plant material was weighed on the STEINBERG SYSTEMS SBS-LW-7500A LCD electronic scale with an accuracy of 0.001 kg.

The depth to which crop residues were incorporated into the soil was determined by measuring uncovered portions of loosened soil after tillage. The depth at which crop residues were placed in soil was measured using a measuring ruler with an accuracy of 0.01 m and measuring instruments. A fragment of uncovered soil measuring 0.3×0.3×0.3 m was selected and three layers were removed from it (0-0.1 m, 0.1-0.2 m, and 0.2-0.3 m). Plant material was separated from each layer using a sieve and were weighed. Crop residues were weighed on the STEINBERG SYSTEMS SBS-LW-7500A LCD electronic scale with an accuracy of 0.001 kg.

Fuel consumption measurements began with a full tank. The fuel tank was completely filled before tillage at the test site. During each refuelling, the tank was vented and the machine was levelled. After refuelling, at least 2.8·10⁴ m² of plot area was tilled by the tractor-pulled aggregated unit. After tillage, the fuel tank was filled to the level determined before the treatment on the same assumptions. Fuel consumption was measured using a graded glass cylinder with an accuracy of 0.002 dm³. Fuel consumption measurements were performed with the use of a system for monitoring the operating parameters of tractor-pulled aggregated tillage units designed and developed by the Department of Vehicle and Machinery Construction and Operation of the University of Warmia and Mazury in Olsztyn. The system relies on GPS technology to determine the duration of the work process, machine status (main and auxiliary operations) and the cultivated area under.

Fuel consumption Q_p per unit of performed work was determined using the following formula:

$$Q_p = \frac{10000 \cdot Q_t}{s_e \cdot a} [\text{dm}^3 \cdot 10^{-4} \cdot \text{m}^{-2}] \quad (2)$$

where:

- Q_t – fuel consumption during cultivation [dm^3],
 s_e – effective distance (when soil is cut by the implement) [m],
 a – the machine's working width [m].

Hourly fuel consumption Q_g was determined using the following equation:

$$Q_g = \frac{Q_t}{t} [\text{dm}^3 \cdot \text{h}^{-1}] \quad (3)$$

where:

- Q_t – fuel consumption during cultivation [dm^3],
 t – duration of tillage [h].

The experimental design is presented in Table 1.

Table 1

Experimental design			
Item	Soil condition	Conducted tests	
1	before tillage	measurement of soil volumetric moisture content (VMC) – 5 measurements	
2		stage 1	determination of the percentage of crop residues that were effectively embedded in the surface layer of soil – 6 measurements
3	after ploughless cultivation*	stage 2	determination of the percentage of crop residues that were effectively embedded in the surface layer of soil – 3 measurements
4		measurement of fuel consumption, beginning with a full tank – 1 measurement	
5		measurement of the depth at which crop residues were incorporated into the soil – 1 test pit	
6	after traditional tillage**	stage 2	determination of the percentage of crop residues that were effectively embedded in the surface layer of soil – 3 measurements
7		measurement of fuel consumption, beginning with a full tank – 1 measurement	
8		measurement of the depth at which crop residues were incorporated into the soil – 1 test pit	

* – tillage involving the MultiCat 6HD aggregated tillage unit

** – two-stage tillage involving a plough and a disc harrow

Results and Discussion

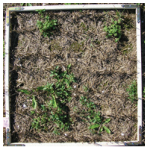



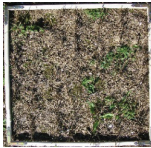

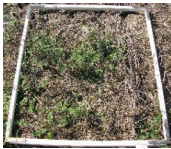





The results of the measurements and the percentage of crop residues that were embedded in the surface layer of soil are presented in Table 2.

The percentage of crop residues that are effectively embedded in the surface layer of soil has a considerable impact on the spread of plant diseases. When infected, non-decomposed residues cover the cultivated soil, pathogens are more likely to be transferred from the residues to the emerging crops, which decreases

yields and increasing spending on plant protection products. The MultiCat 6HD aggregated tillage unit embedded 94.87% of crop residues in soil surface, which is a highly satisfactory result. The above can be attributed to the arched shape of the teeth that dig out soil from deeper layers, as well as disc section No. 3 which evenly distributes the extracted material across the entire field. Ploughless

Table 2

Depth at which crop residues were embedded in the surface layer of soil

Measurement	Before tillage	After tillage	Measurement and calculation results	Average value
No. 1*			$m_p = 1.251 \text{ kg}$ $m_k = 0.052 \text{ kg}$ $R_r = 95.84\%$	$R_r = 94.87\%$
No. 2*			$m_p = 1.376 \text{ kg}$ $m_k = 0.057 \text{ kg}$ $R_r = 95.85\%$	
No. 3*			$m_p = 0.863 \text{ kg}$ $m_k = 0.058 \text{ kg}$ $R_r = 93.27\%$	
No. 1**			$m_p = 1.421 \text{ kg}$ $m_k = 0.014 \text{ kg}$ $R_r = 99.01\%$	$R_r = 99.25\%$
No. 2**			$m_p = 1.155 \text{ kg}$ $m_k = 0.005 \text{ kg}$ $R_r = 99.56\%$	
No. 3**			$m_p = 0.988 \text{ kg}$ $m_k = 0.008 \text{ kg}$ $R_r = 99.19\%$	

* – tillage involving the MultiCat 6HD aggregated tillage unit,
** – two-stage tillage involving a plough and a disc harrow

cultivation and plough tillage produced similar results that differed by only 4.38%, which indicates that soil tillage with the MultiCat 6HD aggregated tillage unit does not differ significantly from plough tillage and creates safe conditions for the growth of crops (by decreasing the risk of pathogen infections).

The depth at which crop residues were incorporated into the soil in the compared cultivation techniques is presented in Table 3. The accumulation

Table 3

Depth at which crop residues were incorporated with soil			
Tillage	Soil layer	Weight	Distribution of plant material
Ploughless cultivation	0-0.1 m	0.15 kg	
	0.1-0.2 m	0.026 kg	
	0.2-0.3 m	0.001 kg	
	material evenly distributed across the entire working width. Plant material evenly mixed with soil		
Plough tillage	0-0.1 m	0.004 kg	
	0.1-0.2 m	0.022 kg	
	0.2-0.3 m	0.138 kg	
	material distributed in strips. Material accumulated at a depth of 0.2-0.24 m		

of plant material in the top soil layer delivers several benefits: it increases the biological activity of soil, promotes the growth of soil-dwelling microorganisms, decreases the loss of soil organic matter, minimizes water and wind erosion, increases soil porosity, reduces soil crusting, and enhances the buffering capacity of soil (SMAGACZ 2013). The conducted analyses demonstrated that plant biomass was accumulated in the top soil layer (0-0.1 m) only in ploughless cultivation. As much as 84.75% of total biomass was evenly distributed in the top soil layer. In contrast, only 2.44% of crop residues were embedded in the top layer (0-0.1 m) as a result of plough tillage, and up to 84.15% of biomass was

Table 4

Results of fuel consumption analysis

Parameter	Ploughless cultivation	Plough tillage	
		Ploughing	Pre-sowing tillage
Duration of tillage	1.3275 h	1.3816 h	0.6132 h
Duration of main operations	1.0938 h	1.1878 h	0.5610 h
Duration of auxiliary operations	0.2337 h	0.1938 h	0.0522 h
Engine crankshaft speed	1,730 rpm	1,730 rpm	1,730 rpm
Transmission ratio	Gear #7	Gear #10	Gear #10
Driving speed	8 km·h ⁻¹	8.8 km·h ⁻¹	8.8 km·h ⁻¹
Average driving speed	7.501 km·h ⁻¹	7.57 km·h ⁻¹	8.52 km·h ⁻¹
Average driving speed during the performance of main operations	7.508 km·h ⁻¹	8.03 km·h ⁻¹	8.49 km·h ⁻¹
Average driving speed during the performance of auxiliary operations	7.46 km·h ⁻¹	4.73 km·h ⁻¹	8.75 km·h ⁻¹
Working width	6 m	3 m	6 m
Working depth	0.4 m	0.22 m	0.12 m
Distance covered	9,958 m	10,466 m	5,225 m
Effective distance	8,213 m	9,548 m	4,768 m
Effective surface area P_e	4.9278 m ²	2.8644 m ²	2.8608 m ²
Effective field capacity W_1	4.5095 [10 ⁴ ·m ² ·h ⁻¹]	2.4115 [10 ⁴ ·m ² ·h ⁻¹]	5.0994 [10 ⁴ ·m ² ·h ⁻¹]
Operational efficiency W_{02}	3.712 [10 ⁴ ·m ² ·h ⁻¹]	2.235 [10 ⁴ ·m ² ·h ⁻¹]	4.665 [10 ⁴ ·m ² ·h ⁻¹]
Fuel consumption during cultivation Q_t	84 dm ³	49.24 m ³	20.53 dm ³
Specific fuel consumption Q_p	17.046 dm ³ ·10 ⁻⁴ ·m ⁻²	17.192 dm ³ ·10 ⁻⁴ ·m ⁻²	7.176 dm ³ ·10 ⁻⁴ ·m ⁻²
Hourly fuel consumption Q_e	63.276 dm ³ ·h ⁻¹	35.639 dm ³ ·h ⁻¹	33.480 dm ³ ·h ⁻¹
Number of passages	27	24	12
Average length of the cultivated plot	304.2 m	397.8 m	397.3 m

speed of the engine crankshaft which was determined at 1,730 rpm in all cases. The same driving speed could not be set at the same rotational speed and at different transmission ratios in the tractors. In conclusion, simplified tillage involving the MultiCat 6HD aggregated tillage unit is far more economical and efficient than plough tillage.

Specific fuel consumption during the field experiment is presented in Figure 4.

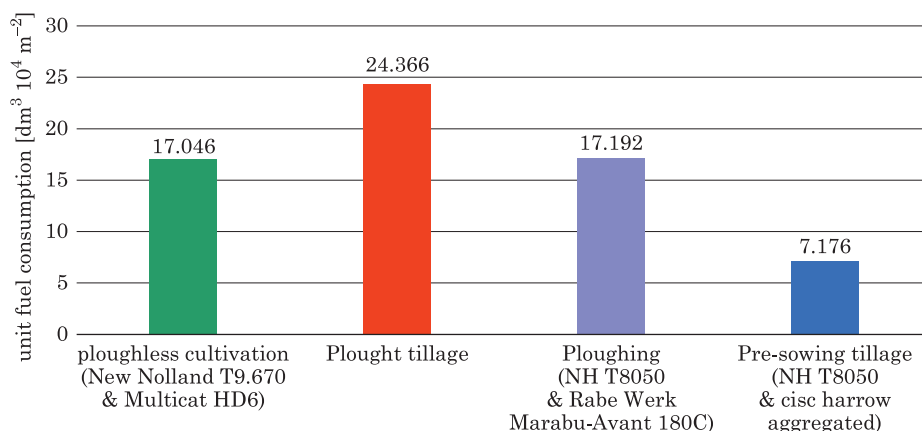


Fig. 4. Specific fuel consumption determined during the field experiment

The average absolute soil moisture content during the field experiment was 15.3% (based on five measurements).

The percentage of crop residues that are effectively embedded in the surface layer of soil was also examined in other studies (ZBYTEK 2010). This parameter was determined at 68% during the cultivation of a stubble field with a tooth-harrow plough (subsoiler, cultivator, discs, string and ring roller), and it ranged from 54% to 81% in ploughless cultivation with an aggregated unit (subsoiler, cultivator, leveller, string roller). These results indicate that the MultiCat 6HD aggregated unit is characterised by superior performance. The depth to which crop residues were embedded in soil by a tooth-harrow plough was identical, but fuel consumption was more than 25% higher in comparison with the MultiCat 6HD aggregated unit.

MOITZI et al. (2006) determined the fuel consumption of a heavy cultivator during ploughless cultivation. Fuel consumption reached $21.55 \text{ dm}^3 \cdot 10^{-4} \cdot \text{m}^{-2}$ at a working depth of only 0.15 m, which is 26% higher than in the MultiCat 6HD aggregated unit.

JASKULSKI and JASKULSKA (2016) measured fuel consumption during ploughless cultivation (grubbing, pre-sowing tillage with an aggregated unit), and the cited values were more than 30% higher on average in comparison with the MultiCat 6HD aggregated unit.

Summary

Ploughless cultivation is a highly promising technology that will gradually replace traditional plough tillage on account of lower energy requirements. Ploughless cultivation and soil loosening to a depth of 0.4 m effectively prevent the formation of a plough pan. The percentage of crop residues that are embedded in the top soil level is similar during ploughless cultivation involving the MultiCat 6HD aggregated tillage unit and traditional plough tillage, which minimizes the risk of pathogen infections in the early stages of plant growth. The above can be attributed to the design of teeth which dig out soil from deeper layers, and the distribution of the excavated material across the entire field by section No. 3 (disc harrow). Crop residues were more favourably distributed within the soil profile by means of ploughless cultivation (84.15% to a depth of up to 0.1 m) which reduces the loss of soil organic matter, minimises water and wind erosion, increases soil porosity, reduces soil crusting, and enhances the buffering capacity of soil. The operating parts of the MultiCat 6HD aggregated tillage unit were not clogged with plant material because biomass was effectively pulverised by a disc section mounted in the front of the tooth section. Simplified tillage involving the MultiCat 6HD aggregated tillage unit reduced fuel consumption by 30% and increased effective field capacity by 63%. The improvement in performance indicators resulting from the application of a new cultivation technology will increase the competitiveness of agricultural farms.

References

- FISZER A., DWORECKI Z., KAŻMIERCZAK P., MORKOWSKI A. 2006. *Comparative analysis of traditional and ploughless cultivation of winter wheat*. Journal of Research and Applications in Agricultural Engineering, 51(3): 23-25.
- GOLKA W., PTASZYŃSKI S. 2014. *Nakłady na uprawę roli w technologii zachowawczej i tradycyjnej*. Problemy Inżynierii Rolniczej, VII-IX(3): 31-47.
- GORYŃSKA-GOLDMANN E., WOJCIESZAK M. 2017. *Program rozwoju obszarów wiejskich 2014-2020 jako źródło podnoszenia innowacyjności*. Roczniki Naukowe Stowarzyszenia Ekonomistów Rolnictwa i Agrobiznesu, XIX(1): 44-51.
- JAKUBOWSKA M., MAJCHRZAK L. 2013. *Wpływ tradycyjnej i bezorkowej uprawy roli na zdrowotność i plonowanie buraków pastewnych*. Fragmenta Agronomica, 30(1): 45–53.
- JASKULSKI D., JASKULSKA I. 2016. *Współczesne sposoby i systemy uprawy roli w teorii i praktyce rolniczej*. Centrum Doradztwa Rolniczego w Brwinowie, Oddział w Poznaniu.
- KASSAM A., FRIEDRICH T., DERPSCH R., KIENZLE J. 2015. *Overview of the worldwide spread of conservation agriculture*. Field Actions Science Reports, 8: 1-11.
- KOSEWSKA A. 2018. *Comparison of ground beetle (Coleoptera, Carabidae) assemblages in tillage and no-tillage cultivation of cereals crop*. Progress in Plant Protection, 58(1): 40-48.
- KUŚ J. 2007. *Uprawa roli w rolnictwie integrowanym. Integrowana produkcja roślinna*. IUNG-BIP, Puławy, p. 135-137.

- MOITZI G., WEINGARTMANN H., BOXBERGER J. 2006. *Effects of tillage systems and wheel slip on fuel consumption*. Energy Efficiency and Agricultural Engineering, International Scientific Conference, 7–9, Rousse, Bulgaria, p. 1-7.
- PIEKARCZYK M. 2006. *Możliwość redukcji dawki herbicydu AFALON 50 WP przy różnej uprawie późniejszej pod łubin wąskolistny*. Acta Sci. Pol., Agricultura, 5(1): 37-44.
- PRZYBYŁ J., KOWALIK I., DACH J., ZBYTEK Z. 2009. *Analysis of the operation quality of aggregates for pre-sow tillage*. Journal of Research and Application in Agriculture Engineering, 54(4): 62-68.
- SEK T., PRZYBYŁ J. 1993. *Wstępna ocena możliwości zmniejszenia energochłonności produkcji buraków cukrowych*. Zeszyty Problemowe Postępów Nauk Rolniczych, 408: 111-117.
- SMAGACZ J. 2013. *Uprawa roli – aktualne kierunki badań i najnowsze tendencje*. In: *Współczesna inżynieria rolnicza – osiągnięcia i nowe wyzwania*. T. III. Eds. R. Hołownicki, M. Kuboń. Polskie Towarzystwo Inżynierii Rolniczej, Kraków, p. 287–329.
- TOPA E. 2020. *The impact of ploughing and zero tillage soil cultivation on species diversity of ground-dwelling spiders in the cultivation of winter rape*. Progress in Plant Protection, 60(3): 247-253.
- ZBYTEK Z. 2010. *Jakość uprawy z zastosowaniem różnych maszyn do dwuwarstwowej uprawy gleby*. Problemy Inżynierii Rolniczej, 1: 63-70.
- ZBYTEK Z. 2010. *Work quality index and energy consumption index for two-layer cultivation and deep plough*. Journal of Research and Applications in Agricultural Engineering, 55(1): 120-123.



SELECTION OF MATERIAL MODEL OF CHOSEN PHOTOCURABLE RESIN FOR APPLICATION IN FINITE ELEMENT ANALYSES

Danuta Miedzińska

ORCID: 0000-0003-2503-6600
Faculty of Mechanical Engineering
Military University of Technology

Received 30 November 2020, accepted 14 December 2020, available online 14 December 2020.

Key words: additive manufacturing, photocurable material, Finite Element Method, constitutive models.

Abstract

In the paper, a literature study of a modelling methods of a photocurable materials developed by additive techniques is presented. The main aim was to assess which material model is appropriate for such kinds of matter. The Finite Element Method and the LS Dyna software was assumed as a possible environment for the investigations. The material models that can be apply for photopolymers analysing were described as well as examples of such materials. The conclusions is that the material model selection must be based on the observation of the material behaviour and the possible loading conditions (e.g. strain rate).

Introduction

The stereolithography (SLA) is one of the additive manufacturing techniques. The main idea of this method is a printing with the use of a photocurable resin, e.g. epoxy or acrylic one. During the crosslinking process the resin is exposed to a ultraviolet (UV) light of a specific wavelength. This physico-chemical process is known as a photopolymerization (DIZON et al. 2018). In practice the SLA

Correspondence: Danuta Miedzińska, Katedra Mechaniki i Informatyki Stosowanej, Wydział Mechaniczny, Wojskowa Akademia Techniczna, 00-908 Warszawa, ul. gen. Sylwestra Kaliskiego 2, e-mail: danuta.miedzinska@wat.edu.pl

is carried out on 3D printers. Such printer working method is presented schematically in Figure 1. The model for the printing is created in a CAD software (Fig. 1a), transformed to STL format (Fig. 1b), divided into slices (Fig. 1c) and printed. The printer is built of a moving platform (1 in Fig. 1d) placed in a tank (2 in Fig. 1d) filled with a liquid polymer (3 in Fig. 1d). The light from an UV laser (4 in Fig. 1d) cures a designed cross-sectional pattern of the sample (5 in Fig. 1d) on the surface of the liquid polymer through a mirror (6 in Fig. 1d). In the next step the platform moves and the curing cycle repeats. The part is built layer by layer of a designed thickness Δz (Fig. 1e), until the object is fully formed (VAEZI et al. 2013).

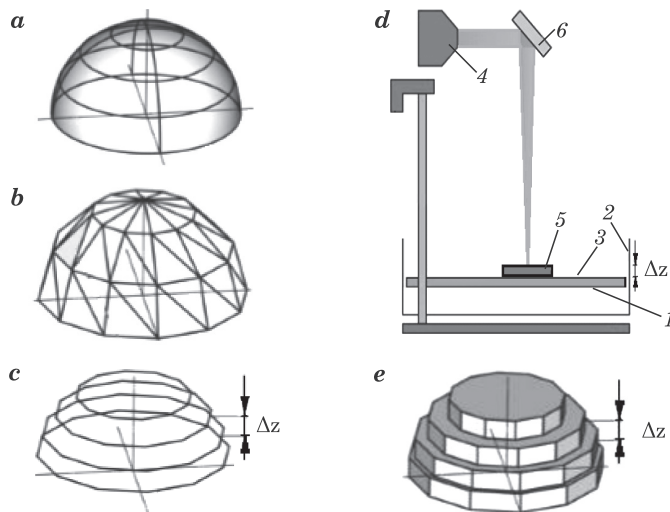


Fig. 1. SLA printing scheme: *a* – CAD model, *b* – STL model, *c* – division into slices, *d* – printer setup (1 – moving platform, 2 – resin tank, 3 – liquid polymer, 4 – UV laser, 5 – printed object, 6 – mirror), *e* – printed model; z – layer thickness

The SLA printed objects can have very complicated shapes, what can be the basis of using it for developing real constructions elements such as energy absorbers or connectors. This idea is also the purpose of designing such elements using finite element method (FEM).

In FEM, a very important problem is to choose and to verify a proper constitutive model for the analyzed material.

In this paper the possible models found in software libraries were reviewed as well as the approaches to such modelling found in the literature. Finally, the numerical analyses of tensile test of a selected SLA resin using different material models was shown.

Numerical approach to polymers modelling – review

Some approaches to numerical modeling of polymers can be found in literature, as well as in calculation software libraries. In the work described in the paper the LS Dyna computer code was used, so the material constitutive models implemented in this software were reviewed and shown below.

The easiest way to model elasto-plastic material, but without considering the chemical changes in polymer chain structure, is to apply the linear plasticity model (in LS Dyna it is *MAT_PIECEWISE_LINEAR_PLASTICITY – MAT_24, HALLQUIST 2007). The material description is based on Young's modulus, Poisson's ratio, yield stress, hardening modulus, ultimate plastic strain, and time step size for element deletion. Also an arbitrary stress versus strain curve and arbitrary strain rate dependency can be defined. In this model deviatoric stresses are determined due to the yield function as:

$$\frac{1}{2}s_{ij}s_{ij} - \frac{\sigma_y^2}{3} \leq 0 \quad (3)$$

The yield stress is calculated as:

$$\sigma_y = \beta \left(\sigma_0 + f_h(\varepsilon_{eff}^p) \right) \quad (4)$$

where:

- β – the strain rate effect parameter,
- $f_h(\varepsilon_{eff}^p)$ – the hardening function,
- ε_{eff}^p – the effective plastic strain.

The other model that can be found in LS Dyna is MAT_168 (*MAT_POLYMER), available since version 971 (HALLQUIST 2007). This model is based on the assessment that the polymer has two resistances to the deformation: an inter – molecular one, related to the relative moment between molecules (*A*), and the other one evolving anisotropic, which is connected to the molecules chains straightening (*B*). This model was is based on the study showed in BOYCE et al. (2000). It can be schematically presented as the mechanical setup built of two springs and a damper (Fig. 2). A resistance of the spring *A* is described on the base of the Neo-Hookean law. On the base of this scheme the deformation gradient tensor is the same for *A* and *B* resistance:

$$\mathbf{F} = \mathbf{F}_A = \mathbf{F}_B \quad (5)$$

and Cauchy stress tensor is a sum of *A* and *B* resistances ones:

$$\boldsymbol{\sigma} = \boldsymbol{\sigma}_A + \boldsymbol{\sigma}_B \quad (6)$$

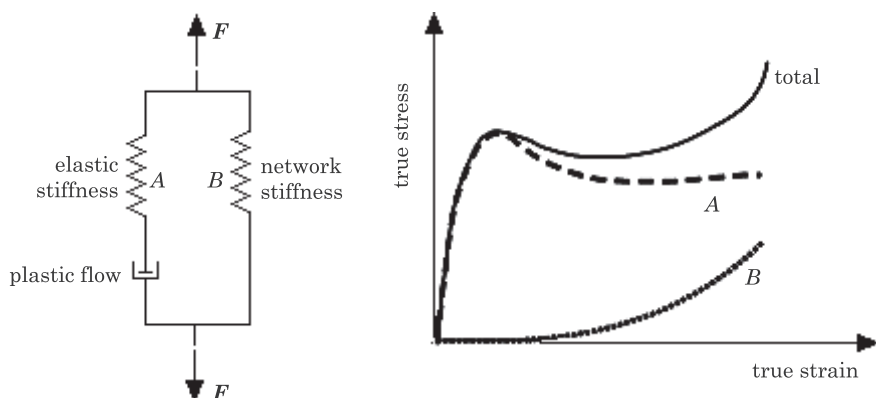


Fig. 2. Schematic illustration of polymers two resistances to deformation: an intermolecular one related to relative moment between molecules (A) and evolving anisotropic one connected with molecules chains straightening (B)

In LS Dyna also the following material models for polymers are available:

- *MAT_081 (MAT_PLASTICITY_WITH_DAMAGE),
- *MAT_089 (*MAT_PLASTICITY_POLYMER),
- *MAT_101 (*MAT_GEPLASTIC_SRATE_2000A),
- *MAT_112 (*MAT_FINITE_ELASTIC_STRAIN_PLASTICITY),
- *MAT_141 (*MAT_RATE_SENSITIVE_POLYMER),
- *MAT_187 (*MAT_SAMP-1).

MAT_081 (HALLQUIST 2007) is the elasto-visco-plastic material description, where stress-strain curve or strain rate dependency can be defined. Damage is considered before rupture occurs. In this model the constitutive properties for the damaged material are obtained from the undamaged material properties. The amount of damage evolved is represented by the constant, ω , which varies from 0 (no damage) to 1 (complete rupture). For the uniaxial loading, the nominal stress, σ_{nominal} , in the damaged material is given as:

$$\sigma_{\text{nominal}} = \frac{P}{A} \quad (7)$$

where:

P – the applied load and A is the surface area.

The true stress is given by:

$$\sigma_{\text{true}} = \frac{P}{A - A_{\text{loss}}} \quad (8)$$

where:

A_{loss} – the void area.

The damage variable is defined as:

$$\omega = \frac{A_{\text{loss}}}{A} \quad (9)$$

In this model damage is defined in terms of plastic strain after the failure strain is exceeded:

$$\omega = \frac{\varepsilon_{\text{eff}}^p - \varepsilon_{\text{failure}}^p}{\varepsilon_{\text{rupture}}^p - \varepsilon_{\text{failure}}^p} \quad \text{if} \quad \varepsilon_{\text{failure}}^p \leq \varepsilon_{\text{eff}}^p \leq \varepsilon_{\text{rupture}}^p \quad (10)$$

MAT_089 (HALLQUIST 2007) describes the elasto-plastic material, for which also stress-strain or strain rate curve can be considered. This model can be applied when the elastic and plastic responses are not clear, as e.g. in metals. Also polymers brittle behavior in high strain rates can be considered. This model is only applicable for 2D elements. MAT_89 is similar to MAT_24 expect the following points:

- loadcurve lookup for yield stress is based on the equivalent uniaxial strain, not the plastic strain;
- elastic stiffness is initial equal to Young modulus but will be increased according to the slope of the stress-strain curve;
- the failure strain depends on the strain rate.

The strain used for failure and damage calculation, ε_{pm} is based on an approximation of the greatest value of maximum principal strain encountered during the analysis:

$$\varepsilon_{pm} = \max_{i \leq n} (\varepsilon_H^i + \varepsilon_{VM}^i) \quad (11)$$

where:

- n – a current time step index,
- $\max_{i \leq n}(\dots)$ – the maximum value attained by the argument during the calculation

and:

$$\varepsilon_H = \frac{\varepsilon_x + \varepsilon_y + \varepsilon_z}{3} \quad (12)$$

where:

- $\varepsilon_x, \varepsilon_y, \varepsilon_z$ – the cumulative strains in the local x, y , and z direction, respectively,

$$\varepsilon_{VM} = \sqrt{\frac{2}{3} \text{tr}(\varepsilon'^T \varepsilon')} \quad (13)$$

where:

- ε' – a deviatoric strain tensor.

MAT_101 (HALLQUIST 2007) is dedicated for thermoplastics. It was developed by General Electric Company to model commercial materials subjected to

high strain rate loading. In this model yield stress is a function of strain rate. This model is described by the constitutive equation:

$$\dot{\varepsilon}_p = \dot{\varepsilon}_0 \exp(A\{\sigma - S(\varepsilon_p)\}) \times \exp(-p\alpha A) \quad (14)$$

where:

- $\dot{\varepsilon}_0$ and A – rate dependent stress parameters,
- $S(\varepsilon_p)$ – internal resistance (strain hardening),
- α – a pressure dependence parameter.

MAT_112 is almost similar to MAT_89, but the elastic response of the model uses a finite strain formulation so that large elastic strains can develop before yielding occurs.

Finally, MAT_141 is a model for isotropic ductile polymers modelling with consideration of strain rate effects. The constitutive equation for the model is as follows:

$$\varepsilon_{ij} = D_0 \exp \left[-\frac{1}{2} \left(\frac{Z_0^2}{3K_2} \right) \right] \left(\frac{s_{ij} - \Omega_{ij}}{\sqrt{K_2}} \right) \quad (15)$$

where:

- D_0 – the maximum inelastic strain rate,
- Z_0 – the isotropic initial hardness of the material,
- Ω_{ij} – the internal stress,
- s_{ij} – the deviatoric stress component,
- K_2 – defined as:

$$K_2 = \frac{1}{2} (s_{ij} - \Omega_{ij})(s_{ij} - \Omega_{ij}) \quad (16)$$

and represents the second invariant of the overstress tensor. The elastic components of the strain are added to the inelastic strain to obtain the total strain. The internal stress variable rate is defined as:

$$\dot{\Omega}_{ij} = \frac{2}{3} q \Omega_m \dot{\varepsilon}_{ij}^I - q \Omega_{ij} \dot{\varepsilon}_e^I \quad (17)$$

where:

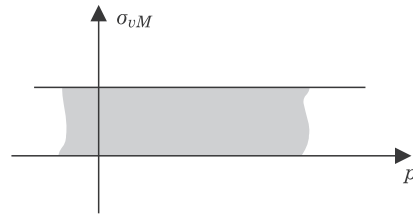
- q – a material constant,
- Ω_m – a material constant that represents the maximum value of the internal stress,
- $\dot{\varepsilon}_e^I$ – the effective inelastic strain.

MAT_187 is a semi-analytical model dedicated for polymeric materials. In this model an isotropic smooth yield surface is implemented for non-reinforced plastics description. Three yield curves are here used and the yield surface has a quadrtic shape. When less then three curves are defined the model calculates the remaining curves as follows (HALLQUIST 2007):

$$\left. \begin{array}{l} \text{LCID_C} = 0 \\ \text{LCID_S} = 0 \\ \text{LCID_B} = 0 \end{array} \right\} \Rightarrow \begin{cases} \sigma_c = \sigma_t \\ \sigma_s = \frac{\sigma_t}{\sqrt{3}} \end{cases}$$

for von Mises cylinder

(18)



or

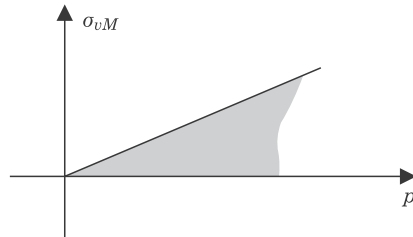
$$\left. \begin{array}{l} \text{LCID_C} = 0 \\ \text{LCID_S} \neq 0 \\ \text{LCID_B} = 0 \end{array} \right\} \Rightarrow \sigma_c = \frac{\sqrt{3}\sigma_t\sigma_s}{(2\sigma_t - \sqrt{3}\sigma_s)}$$

$$\left. \begin{array}{l} \text{LCID_C} \neq 0 \\ \text{LCID_S} = 0 \\ \text{LCID_B} = 0 \end{array} \right\} \Rightarrow \sigma_s = \frac{2\sigma_t\sigma_c}{\sqrt{3}(\sigma_t + \sigma_c)}$$

$$\left. \begin{array}{l} \text{LCID_C} = 0 \\ \text{LCID_S} = 0 \\ \text{LCID_B} \neq 0 \end{array} \right\} \Rightarrow \begin{cases} \sigma_c = \frac{\sigma_t\sigma_b}{(3\sigma_b - 2\sigma_t)} \\ \sigma_s = \frac{\sigma_t\sigma_b}{\sqrt{3}(2\sigma_b - \sigma_t)} \end{cases}$$

for Drucker-Prager cone

(19)



where:

$\sigma_t, \sigma_s, \sigma_c$ – stress values obtained from tensile, shear and compression tests, respectively,

σ_{vM} – von Mises stress,

p – pressure.

The interesting approaches to the modelling of the photocurable polymers can be found in the literature. The scientists use the micro-macro modelling as well as the global one. For example the approach with consideration the micro and macro structure of a printed material using FEM (finite element method) can be found in RODRIGUEZ et al. (2003). The authors applied the elasticity approach to assess the stiffness of ABS material printed with Fused Deposition Modelling (FDM) additive technique. The asymptotic theory of homogenization was applied to predict unidirectional FD-acrylonitrile butadiene styrene material behavior.

In AJOKU et al. (2006) the Nylon printed in SLS (Selective Laser Sintering) technique was modeled using FEM, but the positively validated results were achieved only for the elastic range of the stress. The researched material showed a 7% porosity and voids were placed in the 2D geometric model used for the FE analyses. The authors postulated that the applied geometry is too idealistic to reflect the material behavior in the nonelastic stress rate.

In ZARBAKSH et al. (2015) the sub-modeling approach and FEM were proposed to analyze the mechanical characteristics of 3D-printed parts, whereas the details of 3D printing patterns were included in sub-model.

FEM is not the only method used in modeling the printed materials behavior. In SUGAVANESWARAN and ARUMAICKANNU (2015) the rule of mixture and analytical approach were applied to estimate the elastic properties of the additively manufactured composite parts. The analytical method was validated with the use of the experimental results. The experimental and analytical methods have quite good agreement; hence methodology proposed can be used for estimating the elastic properties of additively manufactured multi material structures.

Another approach was presented in WU (2018), where the evolution of the mechanical properties of the photopolymer during the photocuring process was investigated using theoretical modeling and experimentation. The chemical reaction kinetics was modeled using the first order reaction differential equations.

Chosen photocurable resins description

As it was mentioned the solid sample is developed in the 3D printer using UV light. At the molecular level this process starts from the short chains of photocurable resin, which have active groups in their ends. The resin also includes photoinitiators which exposed to UV light break into two molecules and two radicals. Those radicals are transferred to polymer chains active groups. The chains begin to form longer chains and the liquid resin becomes a solid material. The process was schematically presented in Figure 3 (*The Ultimate Guide...* 2020).

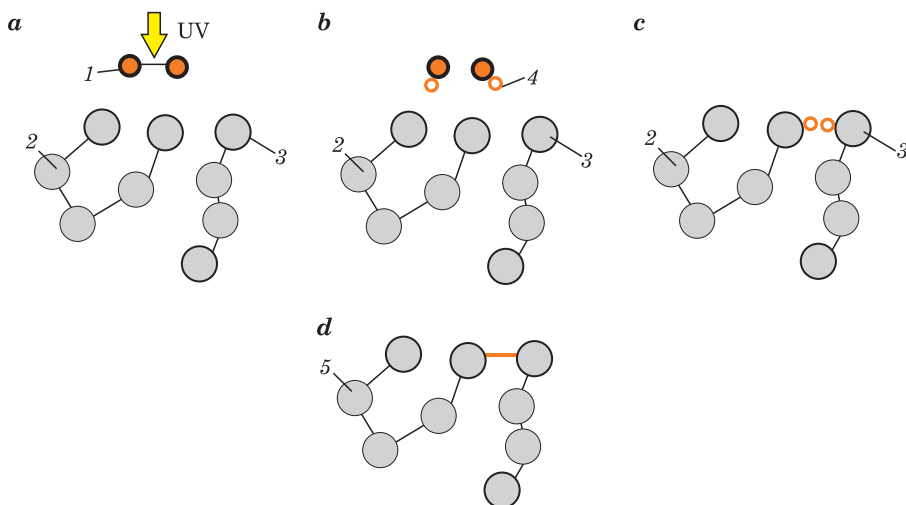


Fig. 3. Scheme of photopolymerization process: *a* – liquid resin short chains and photoinitiator under UV light, *b* – photoinitiator breaks into two molecules and two radicals, *c* – radicals react with polymer chains active groups, *d* – short chains react to create long structure;

1 – photoinitiator, 2 – short chains, 3 – active group, 4 – radical, 5 – long chain

Source: based on *The Ultimate Guide...* (2020).

Currently there are many photocurable resins for the engineering, dental or even jewelry applications. For example the Formlabs company offers the following engineering resins (*Materials Data Sheet...* 2018):

- Grey Pro Resin for high precision printings characterized with moderate elongation, and low creep;
- Tough Resin which handles compression, stretching, bending, and impacts without breaking;
- Rigid 10K - highly glass-filled resin;
- Durable resin highly pliable, impact resistant, and lubricious material.

The mechanical properties of those resins were given in Table 1.

Table 1

Mechanical properties of selected photocurable resins

	Grey Pro resin	Tough resin	Rigid 10K resin	Durable resin
Ultimate tensile strength [MPa]	61	33	55	28
Tensile modulus [GPa]	2.6	15	10	10
Elongation [%]	13	51	1	55

Source: based on *Materials Data Sheet...* (2018).

Summary and conclusions

The models described above were grouped in Table 2 according to their application (type of material, strain rate, elements type etc.).

Table 2

Material models for polymers available in LS Dyna – summary of application

Material model	Application (material type)	Strain rate effect	Failure effect	Damage	Element type	Remarks
1	2	3	4	5	6	7
MAT_24	elasto-plastic materials, metals, plastics, polymers	yes	yes	no	2d, 2d	the most universal model, based on the true stress – true strain curve
MAT_081	elasto-visco-plastic materials considering damage, metals, plastics, polymers	yes	yes	yes	2d, 3d	model based on the true stress – true strain curve
MAT_089	plastics, polymers	yes	no	no	2d	for materials with plastic and elastic sections not clearly separated

cont. Table 2

1	2	3	4	5	6	7
MAT_102	metals, plastics, polymers	yes	no	no	2d, 3d	can be used only after determining the coefficients with the methods only known by GE Company
MAT_112	plastics, polymers	yes	no	no	2d, 3d	for strain rate and temperature dependent plasticity
MAT_141	plastics, polymers	yes	no	no	2d, 3d	for isotropic ductile polymers
MAT_168	plastics, polymers	no	no	no	3d	available since LS Dyna version 971, study of microscopic physical phenomena is needed
MAT_187	plastics, polymers	yes	yes	yes	2d, 3d	available since LS Dyna version 971, no limitations

Source: based on *LS-Dyna Keyword User's Manual* (2012).

On the base of presented review it can be assumed that the model selection should be preceded by at least basic material tests (uniaxial compression and/or tensile test). Then, the analysis of the library of models available in the software should be carried out for the most appropriate reflection of the material properties (e.g. brittleness, thermoplasticity, viscoelasticity, etc., see Tab. 1). Finally the conditions, in which the material will be tested (e.g. strain rate) must be considered. In order to determine the material parameters for the selected model, the necessary experimental tests should be performed. It should also be remembered that each material model must undergo a validation process.

Acknowledgements

The article was written as part of the implementation of the university research grant No. 22-754, MUT, 2020, Warsaw, Poland.

References

- AJOKU U., HOPKINSON N., CAINE M. 2006. *Experimental measurement and finite element modelling of the compressive properties of laser sintered Nylon-12*. Materials Science Engineering A, 428: 211–216.
- BOYCE M.C., SOCRATE S., LLANA P.G. 2000. *Constitutive model for the finite deformation stress–strain behavior of poly(ethylene terephthalate) above the glass transition*. Polymer, 41(6): 2183–2201.
- DIZON J.R.C., ESPERA A.H. JR., CHEN Q., ADVINCULA R.C. 2018. *Mechanical characterization of 3D-printed polymers*. Additive Manufacturing, 20: 44–67.
- EISELE U. 1990. *Introduction to Polymer Physics*. Springer-Verlag, Berlin.
- HALLQUIST J. 2007. *LS Dyna Keyword User's Manual, version 971*. Livermore Software Technology Corporation, Livermore.
- LS-Dyna Keyword User's Manual. 2012. Vol. 2. *Material Models*. Version 971 R6.1.0. Livermore Software Technology Corporation, Livermore.
- Materials Data Sheet: Photopolymer Resin for, Form 1+ and Form 2. 2018. Formlabs. www.formlabs.com, <https://archive-media.formlabs.com/upload/XL-DataSheet.pdf> (access: 12.12.2020).
- MIEDZIŃSKA D., GIELETA R., MALEK E. 2020. *Experimental study of strength properties of SLA resins under low and high strain rates*. Mechanics of Materials, 141: 103245.
- MIEDZIŃSKA D., MALEK E., POPLAWSKI A. 2019. *Numerical modelling of resins used in stereolithography rapid prototyping*. Applied Computer Science, 15(4): 16–26.
- RODRIGUEZ J., THOMAS J., RENAUD J. 2003. *Mechanical behavior of acrylonitrile butadiene styrene fused deposition materials modeling*. Rapid Prototyping Journal, 9(4): 219–228.
- SUGAVANESWARAN M., ARUMAICKANNU G. 2015. *Analytical and experimental investigation on elastic modulus of reinforced additive manufactured structure*. Materials Design, 66: 29–36.
- The Ultimate Guide to Stereolithography (SLA) 3D printing. 2020. Formlabs. www.formlabs.com, https://archive-media.formlabs.com/upload/SLA_Guide.pdf (access: 11.12.2020).
- VAEZI M., SEITZ H., YANG S. 2013. *A review on 3D micro-additive manufacturing technologies*. International Journal of Advanced Manufacturing Technologies, 67: 1721–1754.
- WU J. 2018. *Constitutive modelling of photopolymerization and its application to 3D printing*. Dissertation Presented to The Academic Faculty, Georgia Institute of Technology.
- ZARBAKHSH J., IRAVANI A., AMIN-AKHLAGHI Z. 2015. *Sub-modeling finite element analysis of 3D printed structures*. Proceedings of 16th International Conference on Thermal, Mechanical and Multi-Physics Simulation and Experiments in Microelectronics and Microsystems, Budapest.

Reviewers of Years – book 2020

Mariusz Banaszkiewicz
Ivan Bogdanov
Nicholas Bojdo
Andrzej Chochowski
Tadeusz Chwalczuk
Adam Dacko
Dariusz Dziki
Tadeusz Dziubak
Paweł Flaszyński
Szymon Glowacki
Krzysztof Górski
Monika Gwoździk
Janusz Hetmańczyk
Mark Hlawitschka
Mahmoud Kadkhodaei
Omer Kivanc
Agnieszka Kosewska
Jan Krmela
Leszek Łatka
Danuta Miedzińska

Jerzy Napiórkowski
Bogdan Nedic
Konrad Nowak
Sławomir Obidziński
Mariusz Piekarczyk
Gabriel Nicolae Popa
Norbert Radek
Shafiur Rahman
Grzegorz Redlarski
Bruno Ribeiro
Wojciech Sobieski
Piotr Strzelczyk
Mirosław Szala
Dariusz Szpica
Mikel Tellabide
Piotr Trojanowski
Marek Turzyński
Akarsh Verma
Matthijs de Winter

Guide for Authors

Introduction

Technical Sciences is a peer-reviewed research Journal published in English by the Publishing House of the University of Warmia and Mazury in Olsztyn (Poland). Journal is published continually since 1998. Until 2010 Journal was published as a yearbook, in 2011 and 2012 it was published semiyearly. From 2013, the Journal is published quarterly in the spring, summer, fall, and winter.

The Journal covers basic and applied researches in the field of engineering and the physical sciences that represent advances in understanding or modeling of the performance of technical and/or biological systems. The Journal covers most branches of engineering science including biosystems engineering, civil engineering, environmental engineering, food engineering, geodesy and cartography, information technology, mechanical engineering, materials science, production engineering etc.

Papers may report the results of experiments, theoretical analyses, design of machines and mechanization systems, processes or processing methods, new materials, new measurements methods or new ideas in information technology.

The submitted manuscripts should have clear science content in methodology, results and discussion. Appropriate scientific and statistically sound experimental designs must be included in methodology and statistics must be employed in analyzing data to discuss the impact of test variables. Moreover there should be clear evidence provided on how the given results advance the area of engineering science. Mere confirmation of existing published data is not acceptable. Manuscripts should present results of completed works.

There are three types of papers: a) research papers (full length articles); b) short communications; c) review papers.

The Journal is published in the printed and electronic version. The electronic version is published on the website ahead of printed version of Technical Sciences.

Technical Sciences does not charge submission or page fees.

Types of paper

The following articles are accepted for publication:

Reviews

Reviews should present a focused aspect on a topic of current interest in the area of biosystems engineering, civil engineering, environmental engineering, food engineering, geodesy and cartography, information technology, mechanical engineering, materials science, production engineering etc. They should include all major findings and bring together reports from a number of sources. These critical reviews should draw out comparisons and conflicts between work, and provide an overview of the 'state of the art'. They should give objective assessments of the topic by citing relevant published work, and not merely present the opinions of individual authors or summarize only work carried out by the authors or by those with whom the authors agree. Undue speculations should also be avoided. Reviews generally should not exceed 6,000 words.

Research Papers

Research Papers are reports of complete, scientifically sound, original research which contributes new knowledge to its field. Papers should not exceed 5,000 words, including figures and tables.

Short Communications

Short Communications are research papers constituting a concise description of a limited investigation. They should be completely documented, both by reference list, and description of the experimental procedures. Short Communications should not occupy more than 2,000 words, including figures and tables.

Letters to the Editor

Letters to the Editor should concern with issues raised by articles recently published in scientific journals or by recent developments in the engineering area.

Contact details for submission

The paper should be sent to the Editorial Office, as a Microsoft Word file, by e-mail: techsci@uwm.edu.pl

Referees

Author/authors should suggest, the names, addresses and e-mail addresses of at least three potential referees. The editor retains the sole right to decide whether or not the suggested reviewers are used.

Submission declaration

After final acceptance of the manuscript, the corresponding author should send to the Editorial Office the author's declaration. Submission of an article implies that the work has not been published previously (except in the form of an abstract or as part of a published lecture or academic thesis or as an electronic preprint), that it is not under consideration for publication elsewhere, that publication is approved by all authors and tacitly or explicitly by the responsible authorities where the work was carried out, and that, if accepted, it will not be published elsewhere in the same form, in English or in any other language.

To prevent cases of ghostwriting and guest authorship, the author/authors of manuscripts is/are obliged to: (i) disclose the input of each author to the text (specifying their affiliations and contributions, i.e. who is the author of the concept, assumptions, methods, protocol, etc. used during the preparation of the text); (ii) disclose information about the funding sources for the article, the contribution of research institutions, associations and other entities.

Language

Authors should prepare the full manuscript i.e. title, abstract and the main text in English (American or British usage is accepted). Polish version of the manuscript is not required.

The file type

Text should be prepared in a word processor and saved in doc or docx file (MS Office).

Article structure

Suggested structure of the manuscript is as follows:

Title

Authors and affiliations

Corresponding author

Abstract

Keywords

Introduction

Material and Methods

Results and Discussion

Conclusions

Acknowledgements (optional)
References
Tables
Figures

Subdivision – numbered sections

Text should be organized into clearly defined and numbered sections and subsections (optionally). Sections and subsections should be numbered as 1. 2. 3. then 1.1 1.2 1.3 (then 1.1.1, 1.1.2, ...). The abstract should not be included in numbering section. A brief heading may be given to any subsection. Each heading should appear on its own separate line. A single line should separate paragraphs. Indentation should be used in each paragraph.

Font guidelines are as follows:

- Title: 14 pt. Times New Roman, bold, centered, with caps
- Author names and affiliations: 12 pt. Times New Roman, bold, centered, italic, two blank line above
- Abstract: 10 pt. Times New Roman, full justified, one and a half space. Abstract should begin with the word Abstract immediately following the title block with one blank line in between. The word Abstract: 10 pt. Times New Roman, centered, indentation should be used
- Section Headings: Not numbered, 12 pt. Times New Roman, bold, centered; one blank line above
- Section Sub-headings: Numbered, 12 pt. Times New Roman, bold, italic, centered; one blank line above
- Regular text: 12 pt. Times New Roman, one and a half space, full justified, indentation should be used in each paragraph

Title page information

The following information should be placed at the first page:

Title

Concise and informative. If possible, authors should not use abbreviations and formulae.

Authors and affiliations

Author/authors' names should be presented below the title. The authors' affiliation addresses (department or college; university or company; city, state and zip code, country) should be placed below the names. Authors with the same affiliation must be grouped together on the same line with affiliation information following in a single block. Authors should indicate all affiliations with a lower-case superscript letter immediately after the author's name and in front of the appropriate address.

Corresponding author

It should be clearly indicated who will handle correspondence at all stages of refereeing and publication, also post-publication process. The e-mail address should be provided (footer, first page). Contact details must be kept up to date by the corresponding author.

Abstract

The abstract should have up to 100-150 words in length. A concise abstract is required. The abstract should state briefly the aim of the research, the principal results and major conclusions. Abstract must be able to stand alone. Only abbreviations firmly established in the field may be eligible. Non-standard or uncommon abbreviations should be avoided, but if essential they must be defined at their first mention in the abstract itself.

Keywords

Immediately after the abstract, author/authors should provide a maximum of 6 keywords avoiding general, plural terms and multiple concepts (avoid, for example, 'and', 'of'). Author/authors should be sparing with abbreviations: only abbreviations firmly established in the field may be eligible.

Abbreviations

Author/authors should define abbreviations that are not standard in this field. Abbreviations must be defined at their first mention there. Author/authors should ensure consistency of abbreviations throughout the article.

Units

All units used in the paper should be consistent with the SI system of measurement. If other units are mentioned, author/authors should give their equivalent in SI.

Introduction

Literature sources should be appropriately selected and cited. A literature review should discuss published information in a particular subject area. Introduction should identify, describe and analyze related research that has already been done and summarize the state of art in the topic area. Author/authors should state clearly the objectives of the work and provide an adequate background.

Material and Methods

Author/authors should provide sufficient details to allow the work to be reproduced by other researchers. Methods already published should be indicated by a reference. A theory should extend, not repeat, the background to the article already dealt within the Introduction and lay the foundation for further work. Calculations should represent a practical development from a theoretical basis.

Results and Discussion

Results should be clear and concise. Discussion should explore the significance of the results of the work, not repeat them. A combined Results and Discussion section is often appropriate.

Conclusions

The main conclusions of the study may be presented in a Conclusions section, which may stand alone or form a subsection of a Results and Discussion section.

Acknowledgements

Author/authors should include acknowledgements in a separate section at the end of the manuscript before the references. Author/authors should not include them on the title page, as a footnote to the title or otherwise. Individuals who provided help during the research study should be listed in this section.

Artwork**General points**

- Make sure you use uniform lettering and sizing of your original artwork
- Embed the used fonts if the application provides that option
- Aim to use the following fonts in your illustrations: Arial, Courier, Times New Roman, Symbol
- Number equations, tables and figures according to their sequence in the text
- Size the illustrations close to the desired dimensions of the printed version

Formats

If your electronic artwork is created in a Microsoft Office application (Word, PowerPoint, Excel) then please supply 'as is' in the native document format

Regardless of the application used other than Microsoft Office, when your electronic artwork is finalized, please 'Save as' or convert the images to one of the following formats (note the resolution requirements given below):

EPS (or PDF): Vector drawings, embed all used fonts

JPEG: Color or grayscale photographs (halftones), keep to a minimum of 300 dpi

JPEG: Bitmapped (pure black & white pixels) line drawings, keep to a minimum of 1000 dpi or combinations bitmapped line/half-tone (color or grayscale), keep to a minimum of 500 dpi

Please do not:

- Supply files that are optimized for screen use (e.g., GIF, BMP, PICT, WPG); these typically have a low number of pixels and limited set of colors
- Supply files that are too low in resolution
- Submit graphics that are disproportionately large for the content

Color artwork

Author/authors should make sure that artwork files are in an acceptable format (JPEG, EPS PDF, or MS Office files) and with the correct resolution. If, together with manuscript, author/authors submit color figures then Technical Sciences will ensure that these figures will appear in color on the web as well as in the printed version at no additional charge.

Tables, figures, and equations

Tables, figures, and equations/formulae should be identified and numbered consecutively in accordance with their appearance in the text.

Equations/mathematical and physical formulae should be presented in the main text, while tables and figures should be presented at the end of file (after References section). Mathematical and physical formulae should be presented in the MS Word formula editor.

All types of figures can be black/white or color. Author/authors should ensure that each figure is numbered and has a caption. A caption should be placed below the figure. Figure must be able to stand alone (explanation of all symbols and abbreviations used in figure is required). Units must be always included. It is noted that figure and table numbering should be independent.

Tables should be numbered consecutively in accordance with their appearance in the text. Table caption should be placed above the table. Footnotes to tables should be placed below the table body and indicated with superscript lowercase letters. Vertical rules should be avoided. Author/authors should ensure that the data presented in tables do not duplicate results described in figures, diagrams, schemes, etc. Table must be able to stand alone (explanation of all symbols and abbreviations used in table is required). Units must be always included. As above, figure and table numbering should be independent.

References

References: All publications cited in the text should be presented in a list of references following the text of the manuscript. The manuscript should be carefully checked to ensure that the spelling of authors' names and dates of publications are exactly the same in the text as in the reference list. Authors should ensure that each reference cited in the text is also present in the reference list (and vice versa).

Citations may be made directly (or parenthetically). All citations in the text should refer to:

1. Single author

The author's name (without initials, with caps, unless there is ambiguity) and the year of publication should appear in the text

2. Two authors

Both authors' names (without initials, with caps) and the year of publication should appear in the text

3. Three or more authors

First author's name followed by et al. and the year of publication should appear in the text

Groups of references should be listed first alphabetically, then chronologically.

Examples:

"... have been reported recently (ALLAN, 1996a, 1996b, 1999; ALLAN and JONES, 1995). KRAMER et al. (2000) have recently shown..."

The list of references should be arranged alphabetically by authors' names, then further sorted chronologically if necessary. More than once reference from the same author(s) in the same year must be identified by the letters "a", "b", "c" etc., placed after the year of publication.

References should be given in the following form:

KUMBHAR B.K., AGARVAL R.S., DAS K. 1981. Thermal properties of fresh and frozen fish. *International Journal of Refrigeration*, 4(3), 143–146.

MACHADO M.F., OLIVEIRA F.A.R., GEKAS V. 1997. Modelling water uptake and soluble solids losses by puffed breakfast cereal immersed in water or milk. In *Proceedings of the Seventh International Congress on Engineering and Food*, Brighton, UK.

NETER J., KUTNER M.H., NACHTSCHEIM C.J., WASSERMAN W. 1966. *Applied linear statistical models* (4th ed., pp. 1289–1293). Irwin, Chicago.

THOMSON F.M. 1984. Storage of particulate solids. In M. E. Fayed, L. Otten (Eds.), *Handbook of Powder Science and Technology* (pp. 365–463). Van Nostrand Reinhold, New York.

Citation of a reference as 'in press' implies that the item has been accepted for publication.

Note that the full names of Journals should appear in reference list.

Submission checklist

The following list will be useful during the final checking of an article prior to the submission. Before sending the manuscript to the Journal for review, author/authors should ensure that the following items are present:

- Text is prepared with a word processor and saved in DOC or DOCX file (MS Office).
One author has been designated as the corresponding author with contact details: e-mail address
- Manuscript has been 'spell-checked' and 'grammar-checked'
- References are in the correct format for this Journal
- All references mentioned in the Reference list are cited in the text, and vice versa
- Author/authors does/do not supply files that are too low in resolution
- Author/authors does/do not submit graphics that are disproportionately large for the content